REPORT DOCUMENTATION PAGE

Form Approved
OMB No. 0704-0188

Public reporting burden for this collection of information is estimated to average 1 hour per response, including the time for reviewing instructions, searching existing data sources, gathering and maintaining the data needed, and completing and reviewing this collection of information. Send comments regarding this burden estimate or any other aspect of this collection of information, including suggestions for reducing this burden to Department of Defense, Washington Headquarters Services, Directorate for Information Operations and Reports (0704-0188), 1215 Jefferson Davis Highway, Suite 1204, Arlington, VA 22202-4302. Respondents should be aware that notwithstanding any other provision of law, no person shall be subject to any penalty for failing to comply with a collection of information if it does not display a currently valid OMB control number. **PLEASE DO NOT RETURN YOUR FORM TO THE ABOVE ADDRESS.**

1. REPORT DATE *(DD-MM-YYYY)*	2. REPORT TYPE	3. DATES COVERED *(From - To)*
21 July 2006	Final Performance Report	1 July 2002 to 30 Nov. 2005

4. TITLE AND SUBTITLE
Millimeter Wave Induced BioEffects

5a. CONTRACT NUMBER

5b. GRANT NUMBER
F49620-02-1-0372

5c. PROGRAM ELEMENT NUMBER

6. AUTHOR(S)
Robert Blystone

5d. PROJECT NUMBER

5e. TASK NUMBER

5f. WORK UNIT NUMBER

7. PERFORMING ORGANIZATION NAME(S) AND ADDRESS(ES)

Trinity University
One Trinity Place
San Antonio, Texas 78212

8. PERFORMING ORGANIZATION REPORT NUMBER

9. SPONSORING / MONITORING AGENCY NAME(S) AND ADDRESS(ES)
USAF, AFRL
AFOSR
875 North Randolph Street
Suite 325, Room 3112
Arlington, VA 22203

10. SPONSOR/MONITOR'S ACRONYM(S)

AFRL-SR-AR-TR-06-0329

12. DISTRIBUTION / AVAILABILITY STATEMENT
Unlimited
Approve for Public Release: Distribution Unlimited

13. SUPPLEMENTARY NOTES

14. ABSTRACT

A baseline study determined the conditions of hemodynamic collapse in rats anesthetized with either ketamine plus xylazine or isoflurane alone and exposed to environmental heat at 42 or 43°C, 35 GHz at 75 or 90 mW/cm^2, or 94 GHz at 75 or 90 mW/cm^2. Focusing on continuous 94 GHz exposures at power densities of 50, 75, or 100 mW/cm^2, at 23 or 33°C ambient, for 15, 30, 45, and 60 minutes administered to the left abdominal flank of male rats, the temperature response at the skin surface, subcutaneous, and core were coordinated with exposed skin histology. Four anatomical injury threshold responses were defined: panniculus carnosus muscle change @ 42.1°C, dermis blood vessel dilation @ 42.9°C, extravasation @ 42.9°C, and epidermal blistering @ 44.1°C. Progressive skin injury was apparent at 100 mW/cm^2 but not 50 mW/cm^2 with 75 mW/cm^2 intermediate. A 10°C ambient elevation during exposure dramatically increased skin injury. Anesthesia depressed rat body temperature response and masked exposure response by about 2°C. The Gaussian nature of MMW delivery was explored through a coordinated thermograph/histology investigation. Steps were taken to model heat flow through the skin. Thermoregulation of hyperthermic skin was explored.

15. SUBJECT TERMS
Millimeter wave exposure, skin histology and pathology, thermal modeling, thermoregulation

16. SECURITY CLASSIFICATION OF:			17. LIMITATION OF ABSTRACT	18. NUMBER OF PAGES	19a. NAME OF RESPONSIBLE PERSON
a. REPORT unclassified	**b. ABSTRACT** unclassified	**c. THIS PAGE** unclassified	none	62	Robert Blystone
					19b. TELEPHONE NUMBER *(include area code)* 210 999 7243

Standard Form 298 (Rev. 8-98)
Prescribed by ANSI Std. Z39.18

FINAL PERFORMANCE REPORT

Principal Investigator: Robert V. Blystone, Ph.D.
                             Dept. of Biology
                             Trinity University
                             One Trinity Place
                             San Antonio, Texas 78212
                             210-999-7243 (Voice)
                             210-999-7229 (Fax)
                             rblyston@trinity.edu

1. **Objectives:**
    a. **Objective 1:** *Develop mathematical dosimetry models to predict temperature changes occurring in skin and subcutaneous tissue during MMW exposures.*
    b. **Objective 2:** *Determine time-to-death during exposure to MMWs, environmental heat, and environmental heat + infrared heat. Infrared heating is added to the environmental heat in order to warm the dermis and subcutaneous tissue to levels similar to those during MMW exposure. Core temperature profiles are matched for all exposures. Measure nitration products immediately following death.*
    c. **Objective 3:** *Determine time-dependent changes in gene and protein expression, nitration products, expired air, and skin pathology following less-than-lethal exposures to MMWs, environmental heat, and environmental heat + infrared heat.*
    d. **Objective 4:** *Based on the data revealed by Objective 3, focus on specific mechanisms, as well as, develop clinical biomarkers of prolonged MMW exposure.*
    e. **Objective 5:** *Pharmacological modulation of specific genes, proteins, and nitration pathways to prevent early death from occurring during prolonged MMW exposure.*
    f. **Objective 6:** *Determine time-dependent changes in gene and protein expression, nitration products, and skin pathology following brief (<10 sec) MMW exposures (> 1 W/cm^2).*
    g. **Objective 7:** *Based on the data revealed in Objective 6, focus on specific mechanisms, as well as, develop clinical biomarkers of brief MMW exposures.*

20060804052

2. **Status of Effort:**
    a. **Objective 1:** J. Weaver (through the grant subcontract) developed a "crystalline lattice" model for predicting temperature changes. The modular model represented an effort to fit both continuous wave and pulsed wave exposures. The effort has been incorporated into a publication. Dr. Blystone contacted Dr. David Nelson of Michigan Tech and a collaborative effort was undertaken to develop a 2-D Finite-Difference Time Domain Model to predict energy flow and temperature change in skin. Dr. Nelson has developed some initial models and a synopsis is a part of this report.
    b. **Objective 2:** Dr. Millenbaugh et al. has published the results of the time-to-death study.
    c. **Objective 3:** Dr. Mason's research group through separate funding is now addressing this objective.
    d. **Objective 4:** Blystone initiated during the late summer of 2004 specific mechanism experiments that explored the effect of different ambient environments, power density, and passive heating on animal/exposure interaction. The results of those experiments are the primary focus of this report. The results directly impact Objective 1 above, the modeling of energy flow and heat distribution in the skin.
    e. **Objective 5:** Based on earlier data we have not continued this line of investigation.
    f. **Objective 6:** Minimal progress was made toward this objective.
    g. **Objective 7:** No progress has been made towards this objective. The majority of the research period was spent on long duration, lower power density exposures.
3. **Scientific personnel supported by this grant along with their percent effort:**
    a. Adam Back (Undergraduate Research Student) – 25% Fall 2004, Spring 2005, and Fall 2005, 100% Summer 2005.
    b. Robert V. Blystone, Ph.D. (Principal Investigator) – 100% summer, 100% fall term of academic year, 20% spring term of academic year.
    c. Becky Brott (Research Technician II) - 100% June 1, 2003 through June 1, 2005 (left project to attend medical school).
    d. Fernando Catalan (Research Technician I) – 100% July 1, 2004 through May 1, 2005 (left project to attend medical school).
    e. Cesario Cerna (Research Technician II) – 100% June 15, 2003 through December 31, 2004.
    f. Jacqueline Crissey (Undergraduate Research Student) – 20% Fall 2003 and Spring 2004.
    g. William Lawrence (Research Technician) – 100% - left project mid-June 2003.
    h. Marcos Lopez (Undergraduate Research Student) – 25% Spring 2005 and Fall 2005, 100% Summer 2005.
    i. Richard McLaughlin (Undergraduate Research Student) – 100% Summer 2003, 25% Spring 2003, 100% Summer 2004.
    j. Juliana Robles (Research Technician I) – 100% June 1, 2005 through November 30, 2005.
    k. Carlos Roldan (Undergraduate Research Student) – 50% Summer 2005 through Fall 2005.
    l. Ryan Scholz (Undergraduate Research Student) – 25% Spring 2003, 100% Summer 2003, 20% Fall 2003 and Spring 2004.

   m. Laura Soza (Research Technician) – 100% - left project May 2003.
   n. Roza Sypniewska (Research Scientist) – 100% (most salary paid through Veridian).
   o. Denise Wilson (Research Assistant) – 35% March 22, 2004 through November 30, 2005.

4. **List of Manuscripts Submitted/Published:**
   a. *Comparison of blood pressure and thermal responses in rats exposed to millimeter wave energy or environmental heating.* Millenbaugh, N., J. L. Kiel, K. L. Ryan, R. V. Blystone, J. Kalns, B. Brott, C. Cerna, W. Lawrence, L. Soza, and P. Mason. (2006). Shock, 25: 625-632.
   b. *Skin heating and injury by prolonged millimeter wave exposure: theory based on a skin model coupled to a whole body model and local biochemical release from cells at supraphysiologic temperatures.* Stewart, D. A., J. R. Gowrishankar, and J. C. Weaver. (2006). IEEE Transactions on Plasma Science, 34(4):1-13.

5. **Interactions/Transitions:**
   a. **List of Peer-Reviewed Presentation/Abstracts:**
      i. *Proteomic assessment of macrophage activation in plasma bioassay.* R.Sypniewski, N..J. Millenbaugh, C. Cerna, B. Brott, J.L. Kiel, R.V. Blystone, H. Coppage, F. Witzmann, and P.A. Mason World Health Organization: Workshop on Application of Proteomics and Transcritomics in EMF Research, Helsinki, Finland, October 31, 2005.
      ii. *Mammalian skin response to 94 GHz applied at 50 to 200 mW/cm2 for up to 60 minutes.* R. Blystone, F. Catalan, J. Robles, A. Back, M. Lopez, C. Roldan, and N. Millenbaugh. 12th annual Michaelson Research Conference, Hood River, Oregon, July 30, 2005.
      iii. *Gene expression changes in skin of rats exposed to sustained 35-GHz radio frequency radiation.* N.J. Millenbaugh, R. Sypniewska, C.C. Roth, J.L. Kiel, R.V. Blystone, and P.A. Mason. 27th Annual Meeting of the Bioelectromagnetics Society, Dublin, Ireland, June 21, 2005.
      iv. *Visualization of millimeter wave effects on mammalian skin.* R. Blystone, R. Scholz, F. Catalan, J. Eggers, N. Millenbaugh, R. Sypniewska, J. Kalns, J. Kiel, and P. Mason. 26th annual meeting of the Bioelectromagnetics Society, Washington, D.C., June 23, 2004.
      v. *Integrated approach to millimeter wave biomarker discovery.* N.J. Millenbaugh, R. Sypniewski, J.E. Kalns, P.A. Mason, J.S. Eggers, R.V. Blystone, and J.L. Kiel. 26th annual meeting of the Bioelectomagnetics Society, Washington, D.C., June 22, 2004.
      vi. *Nitration pathways activated in macrophage cells treated with plasma from 35GHz MMW exposed rats.* R. Sypniewska, J. Kiel, N. Millenbaugh, J. Kalns, R. Blystone, P. Mason. C. Cerna, B. Brott, M. Tarango, H. Coppage, N. Pedrick, J. Tan, and F. Witzmann. 26th annual meeting of the Bioelectromagnetics Society, Washington, D.C., June 22, 2004.
      vii. *Use of proteomics and HPLC to screen plasma for markers of millimeter wave overexposure.* J.L. Kiel, N.J. Millenbaugh, R. Sypniewska, J.E. Kalns, R.V. Blystone, P.A. Mason, L.L. Soza, and W.S. Lawrence. Presentation and abstract to the 12th International Congress of Radiation Research, Brisbane, Australia, August 18, 2003.

viii. *Pathology of rat skin following prolong millimeter wave exposure.* J.S. Eggers, R.V. Blystone, N.J. Millenbaugh, J.E Kalns, P.A. Mason, J.L. Kiel, L.L. Soza, and W.S. Lawrence. Presentation and abstract to the 25th annual meeting of the Bioelectronmagnetics Society, Maui, Hawaii, June 25, 2003.

ix. *Comparison of vascular and thermal responses in rats exposed to prolonged millimeter wave or environmental heating.* N.J. Millenbaugh, R.V. Blystone, J.E. Kalns, P.A. Mason, L.L. Soza, W.S. Lawrence, J.S. Eggers, C.T. Kuhnel, L.R. Johnson, and J.L. Kiel. Presentation and abstract to the 25th annual meeting of the Bioelectromagnetics Society, Maui, Hawaii, June 23, 2003.

x. *Exposure to 35 GHz millimeter wave energy (MMW) causes changes in expression of heat-shock protein (HSP-27).* R. Sypniewska, J.E. Kalns, P. Mason, N. Millenbaugh, L.L. Soza, W. Lawrence, R. Blystone, J. Eggers, and J.L. Kiel. Presentation and abstract to the 25th annual meeting of the Bioelectromagnetics society, Maui, Hawaii, June 23, 2003.

xi. *Identification of biomarkers of millimeter wave overexposure using proteomics and high pressure liquid chromatography ((HPLC).* N.J. Millenbaugh, R. Sypniewska, J.E. Kalns, P.A. Mason, L.L. Soza, W.S. Lawrence, J.S. Eggers, J.L. Kiel, and R.V. Blystone. Presentation and abstract to the Electromed 2003 Conference, San Antonio, Texas, June 13, 2003.

b. **Collaborators/Consultants:**

i. Col. Jeffrey S. Eggers, Chief, Comparative Pathology, AFRL/HEDV, Brooks City Base. Dr. Eggers provides pathology support for our efforts. He greatly contributes to our research discussions.

ii. Dr. John M. Frazier, Senior Scientist, AFRL/HEST, Wright-Patterson Air Force Base, Ohio. Dr. Frazier's lab is performing genomic readouts of prepared tissue samples from our exposed animals in order to identify potential biomarker candidates.

iii. Dr. Johnathan Kiel, Senior Scientist, AFRL/HEDB, Brooks City Base, Texas. Dr. Kiel heads a research group that investigates the cellular responses to 35 and 94 GHz, which directly supports and compliments our efforts at the animal level. Both co-PI's are members of Dr. Kiel's research team. Our research efforts are tightly coordinated.

iv. Dr. Patrick Mason – Research Physiologist, AFRL, HEDR, Brooks City Base, Texas. Dr. Mason serves as the liaison of HEDR for this grant. He provides support in terms of exposure equipment, lab space, animal facilities, and office space. He participates in our research meetings and keeps us mindful of the Air Force mission. Dr. Mason is the P.I. of a companion research effort funded through AFOSR.

v. Dr. Nancy Millenbaugh – Scientist, General Dynamics, Brooks City Base, Texas. Dr. Millenbaugh was previously a co-PI on this grant. She is now working principally on a companion effort funded through AFSOR with Dr. Patrick Mason as P.I. Her focus is on the genomics and proteomics of possible biomarkers induced by MMW.

vi. Dr. David A. Nelson – Professor of Engineering, Michigan Technological University, Houghton, Michigan. Dr. Nelson is developing a computational

skin model of energy and heat transfer based on dimensional information provided by my research team. His primary approach to the problem is via FDTD (finite-difference time domain) algorithms. Dr. Nelson has a long history of collaboration with Dr. Mason.

vii. Dr. Terence H. Risby, Professor, School of Hygiene and Public Health, Johns Hopkins University, Baltimore, MD. Dr. Risby has conducted feasibility experiments in an effort to identify a potential biomarker in the breath of exposed animals.

viii. Dr. Roza Sypniewska, Scientist, General Dynamics, Brooks City Base, Texas. Dr. Sypniewska was previously employed directly by this grant but is now employed by General Dynamics. She is a participant in a companion effort funded through AFSOR with Dr. Patrick Mason as P.I. Her focus is on the genomics and proteomics of possible biomarkers induced by MMW.

ix. Dr. James C. Weaver, Associate Director, HST Biomedical Engineering Center, MIT, Cambridge, MA. Dr. Weaver and his associates are building mathematical models of energy flow through modeled skin.

x. Dr. Frank A. Witzmann, Prof. of Cellular & Integrative Physiology, School of Medicine, Indiana University, Indianapolis, IN. Dr. Witzmann analyzed rat macrophage nitrated proteins activated after exposure to MMW and EH in order to determine the effect this plasma on the activation status of rat macrophages.

c. **Transitions:**   None
6. **New Discoveries, inventions, or patent disclosures:**   None
7. **Honors and Awards:**   None
8. **The technical report follows.**

Preamble: With the reorganization of the two research teams, the BioEffects research team refocused on seven objectives.

A). Relationship of Power Density to tissue response to 94 GHz
B). Exposure time variation and recovery time variation to 94 GHz
C). The effect of ambient temperature on exposure response
D). The effect of anesthesia on exposure response
E). Passive heating effects
F). Thermograph correlation to histology
G). Modeling MMW induced heat flow through skin

Introduction:
Prepared for objective A.

Skin consists of three functionally and anatomically different layers: epidermis, dermis, and hypodermis (also called subcutaneous). The thin epidermis demonstrates various living and dead cell layers. The much thicker dermis is traditionally divided into papillary dermis (just below the epidermis) and reticular dermis (a larger zone above the hypodermis). The hypodermis is primarily a mixture of adipose and muscle layers. The muscle layer closest to the dermis is called the panniculus carnosus (note that this layer has different names at different body locations and varies from species to species). Although the panniculus carnosus muscle focused on in our study is readily found in rats and to a lesser degree in humans, it can be expected that skeletal muscle in general will likely respond in similar methods. The anatomy of the skin is highly variable depending on body location. In addition, non-glabrous (haired) skin anatomy may vary at a specific location based on where in time the skin is in the hair cycle [Chase et al. 1953]. Generally the average thickness of mammalian haired skin ranges from as little as 0.5 mm to 5 mm, again depending on location and of the species being considered. In addition, Thomas [2005] suggested that aging and caloric restriction have an effect of the skin histology of the rat. It is thus important to have an understanding of the effects of age, weight, and location of exposure in order to understand the effects of MMW under more universal conditions.

MMW interaction with the skin has a primary effect of increasing the temperature of the exposed region through increasing the vibrations of atoms and molecules such as proteins, DNA, and lipids according to [Erwin 1983; Xiao-feng and Anying 2003]. The electromagnetic energy is converted into mechanical or rotational energy, which eventually is turned into heat energy causing a temperature rise in exposed tissue. It is important to appreciate how MMW heats tissue in order to understand how increasing MMW power density affects the thermal conditions of the tissue.

Thermoregulation is the term that is applied to the ability of the body to maintain temperature within a set temperature range even when thermal conditions may not be constant [Adair and Black 2003]. When an animal can no longer regulate the thermal stresses applied to it, injury response can occur. Our study suggests the primary thermoregulatory response is to distribute the heat via circulation; a view that is also supported in Gordon's review [1990] in which he examines several aspects of the thermal biology of a rat.

Nelson et al. [2000] described the extent of local temperature rise being primarily affected by conduction of heat to surrounding regions, distribution of heat via circulation, and convection of heat from the skin surface. Diller and Ryan [1998] also examined the transfer of heat in living systems including different sources of thermal heat and examine models of heat

transfer. Ferguson et al. [1982] and Aulick et al. [1978] found that thermal injury results in the increase in arteriolar circulation in muscle regions. In our study the panniculus carnosus muscle atrophied, despite being deeper than the suggested penetration depth of 94 GHz MMW, suggesting that the vascular system plays a large role in the distribution of heat during MMW exposure. Alekseev et al. [2005] showed that tissue heating occurs in layers located deeper than the penetration depth of the MMW suggesting the influence of perfusion in heat distribution. Nelson et al. [2000] showed that increased blood perfusion reduces the maximum surface temperature response to MMW exposure of a primate scalp model at 100 GHz. Our study also shows that the rate of surface temperature decreases after a period of time in response to the distribution of heat via the circulation to the body core. The ability of the animal in our study to manage the excess heat provided by the MMW exposure determined the extent to which tissue injury was observed.

Although rats serve as a predictive model for human response to MMW it must also be noted that humans are anatomically and physiologically unique. Adair and Black [2003] suggested that humans are more efficient and effective in thermoregulation in response to MMW exposure as compared to other species. Charkoudian [2003] described the thermoregulatory ability of adult humans including the physiological and neurological control mechanisms. Rats are known to have sweat glands like human; however, rats only have them in the paw region of the animal and also unlike humans is not believed to be involved in the thermoregulatory effect of the animal [Gordon 1990]. In addition the surface area to volume ratio of the rat is much higher than humans.

A primary mechanism a rat uses to thermoregulate is via the distribution of heat through the vascular system towards the tail. The rat tail acts as a major site of heat exchange with extensive circulatory elements present in the tail including a dorsal vein, two lateral veins, and a ventral artery [Weiss et al. 2000]. It has been suggested that 20% of the total heat production under normal conditions is dissipated by the tail [Rand et al. 1965; Young and Dawson 1982]. The tail is has a large surface area exposed to the ambient environment and is a highly vascularized surface without coarse hairs allowing for heat convection to the environment. In objective C we examined the effects of ambient temperature on rat thermoregulation in response to 94 GHz MMW exposures. An understanding of the effects of ambient temperature on tissue injury response can enhance an appreciation of the regulatory role of the tail. Dawson and Keber [1979] found that the tail of the rat is controlled in an on/off mechanism in heat regulation involving blood vessel dilation.

Jauchem et al. [1999] described circulatory collapse in a rat that occurs after a period of time in response to 94 GHz 75 mW/cm^2 MMW. Heat transfer occurred initially in the periphery of the animal and was then transferred to the core causing the mean arterial pressure of the animals to begin falling after 10 minutes of exposure. In addition the heart rate of the animal increased over the entire exposure period. Clearly the cardiovascular system of the animal is highly responsive to MMW exposure and should be a part of any study involving MMW exposure. The animals in their study survived for 40 minutes of exposure before experiencing a circulatory failure. In our study the animals lasted for sixty minutes despite similar exposure conditions. A difference between the two studies is Jauchem et al. used a ketamine injection anesthetic while our study used gas isoflurane.

The energy associated with 94 GHz MMW is absorbed primarily by the skin. It is increasingly important to understand how MMW interacts with skin and how heat associated with MMW energy in the skin moves in living tissue. The goal of objective A was to record the

skin injury response to 94 GHz at power densities at 50, 75, and 100 mW/cm^2. In order to understand skin tissue response at these three power densities digital histological images were obtained and examined after exposure. Injury responses to exposures were recorded and temperature thresholds for the injuries were also obtained. In addition our study focused on identifying temperature threshold levels for injury response in skin tissue.

Prepared for objective B.

The body penetration depth at millimeter-wave frequencies is less than 1 mm, with the resultant primary effect of exposure of surface heating and anatomical changes in the skin [Nelson et al. 2000; Adair and Petersen 2002; Pakhomov et al. 1998]. However, studies on rodent models have shown significant subcutaneous and core body heating from prolonged, continuous exposure to 75 mW/cm^2 at frequencies of 35 GHz and 94GHz [Millenbaugh et al. 2006; Frei et al. 1995; Jauchem et al.,1999; Nelson et al. 2000]. Many of the studies reporting unexpected bioeffects in deeper tissues have concentrated on continuous exposure to MMW at different power densities and for a specified amount of time [Millenbaugh et al. 2006; Gordon and Ali 1987]. For example, Millenbaugh et al. [2006] have defined the time-to-death parameters of the lethal continuous application to rodents of 35 and 94 GHz at power densities of less than 100 mW/cm^2 and at 23°C. While most recent studies give an excellent idea of the overall bioeffects at the end of a long exposure and further support that deeper tissues are altered by MMW, they may tell us nothing about the path of injury, time and energy needed to reach a certain point of change, heat flow through time and at specific time periods, and whether heat load and injury are handled in a gradient or a threshold style of change in physiology and anatomy.

MMW bioffects in deeper tissues suggest that the primary response in the skin mediates subsequent reactions into the body by blood flow and/or neural pathways [Walters et al. 2004; Xiao-feng and Anying 2003; Gowrishankar et al. 2004; Alekseev et al. 2005]. Thus, building upon the experience of previous work, we have explored variations in tissue response after different exposure lengths of potentially lethal power densities of 94 GHz MMW and after a 1, 2, or 3 day recovery period. The goal of objective B was to define histological changes and corresponding physiological data at fifteen-minute intervals of a 60-minute exposure so as to reveal a larger picture of heat flow and heat loss through the body. To elucidate long-term response to exposure, skin tissue was also examined after defined recovery intervals.

Prepared for objective C.

One of the primary effects of MMW exposure is the creation of heat in a living organism, thus the ambient temperature during exposure could have a substantial role in response to MMW energy [Adair et al. 1985; Gordon and Ali 1987; Jauchem et al. 1999; Xiao-feng and Anying 2003]. The exposures carried out in this study were approximately 1000 times the limit recommended by IEEE C95.1-2005. The effects of ambient temperature on prolonged, high power density exposure to 94 GHz energy have not previously been examined.

The thermoneutral zone for rats is defined as the temperature range at which temperature is regulated primarily through the modulation of peripheral motor tone and non-evaporative heat loss. The upper critical temperature, the ambient temperature above which an animal recruits evaporative mechanisms for heat loss, for rats has been defined at approximately 33°C [Gordon 1990]. Gordon [1990] also notes that at lower temperatures heat can be dispersed through radiation, convection, and conduction. Physiological responses such as vasodilation can be

activated to enhance these mechanisms of heat loss. Nelson et al. [2000] noted that increased blood flow acted to reduce the rate of temperature rise caused by MMW exposure. At higher ambient temperatures, the mentioned mechanisms are no longer effective because of the reduced gradient between skin and environmental temperatures [Jauchem et al. 1999]. Rats exposed to MMW energy at an ambient temperature of 33°C would not be able to recruit vasodilatation and increased skin blood flow as effective responses to heat added from exposure as would rats exposed in the thermoneutral zone. This impaired heat response in 33°C exposed rats would, in turn, likely lead to a higher level of injury in exposed tissue. It has been reported that high body core temperature is related to circulatory failure and subsequent expiration of animals exposed to MMW energy over prolonged periods [Frei et al. 1995; Jauchem et al. 1999; Millenbaugh et al. 2006]. The time-to-death associated with increased body core temperature leading to circulatory failure should then be reduced as a result of the decreased ability to shed heat at higher ambient temperatures.

A comparison of heat buildup in animals exposed to MMW at different ambient temperatures can be used to estimate heat loss in the animal at a lower ambient temperature. That is, the difference between the presumed faster heat buildup in animals exposed at 33°C and that of animals exposed at the standard ambient temperature of 23°C would give an estimate of heat loss from the body at 23°C. Through histology and measured temperature changes, objective C aims to further define the role played by ambient temperature in heat accumulation and regulation in animals exposed to MMW energy for prolonged periods.

Prepared for objectives D and E.

In a thermal sense the body is divided into two compartments that are almost equally divided in terms of body mass: core and peripheral. [Sessler 2000] In Sessler's review based primarily on human data, the body core is generally from 2 to 4 degrees warmer than the peripheral compartment, which includes arms, legs, and skin. Heat loss from the body involves radiation, conduction, convection, and evaporation. Heat loss from the core is based on the morphometry of the subject with the vasoconstriction process being similar across body types. (Kurz et al. 1995] Most studies involving heat flow in the body consider heat movement outward. Our work involves heat flow inward. There is an interesting convergence: anesthesia causes vasodilation and loss of heat from the body. In humans the heat loss is between 1 and 1.5°C during the first operative hour. [Sessler 2000]. Lenhardt et al. [1999] records that in humans the skin can be responsible for 20% of the heat movement in the body. Does our rat model respond to the isoflurane anesthesia by loosing temperature? An experiment was devised to describe anesthesia temperature loss while the anesthetized rat was being heated by MMW.

Charkoudian [2003] recently reviewed regulatory elements of skin blood flow: "Sympathetic neural control of skin blood flow includes the noradrenergic vasoconstrictor system and a sympathetic active vasodilator system, the latter of which is responsible for 80% to 90% of the substantial cutaneous vasodilation that occurs with whole body stress." Jauchem [2006] has explored the role of autocoids and the autonomic nervous system in cardiovascular responses to radio-frequency energy heating. To explore the heat flow in rat skin, an alternate approach was taken. We monitored heat movement in exposed dead animals where neither blood flow nor nervous system involvement plays a role in the movement of MMW generated heat. We combined this study with that of the heat support for cooling due to anesthesia. This experiment was called the passive heating trial.

Prepared for objective F.
      The figure below provides an insight that has driven the thermograph study. The anatomy
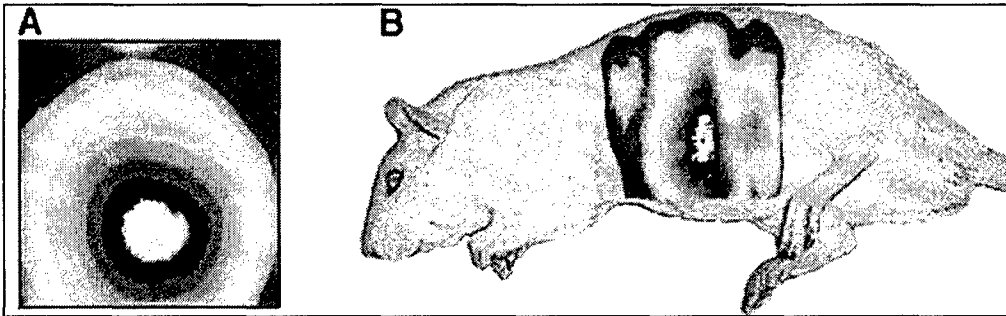

Figure 1: Comparison of calibration thermograph on flat field (left) with same exposure on animal (right).

of the animal greatly affects the distribution of surface temperature. A question was provoked by this distribution pattern: does the skin histology underlying the surface temperature reflect the temperature variation pattern seen on the surface? A thermograph correlation to histology experiment was designed.

Methodology:
      At the onset of this research project several parameters had to be defined: 1) the best exposure conditions to produce tissues that could be used to seek biomarkers to exposure; 2) the best methods to handle the experimental animal; and 3) the best methods to collect histological samples and analyze images taken from those tissues. Parameter 1 and 2 were primarily satisfied by research led by Dr. Millenbaugh and recently published in Shock [Millenbaugh et al. 2006]. Her groups' work was referred to as "the time to death" study.
      Historically our lab had used ketamine as the anesthetic of choice. (Frei et al. 1995). As we became more aggressive in exploring exposure conditions we moved to a combination of ketamine and xylazine. In a previous AFOSR grant this combination anesthetic proved successful. However, as the research moved towards recovering animals after exposure, the ketamine and xylazine had undesirable effects on the tissue. We migrated to isoflurane as the anesthetic of choice and repeated the time-to-death work that had been done with the combination drug. Examples of the results are seen in the figures below (taken from the Millenbaugh et al. 2006) paper.
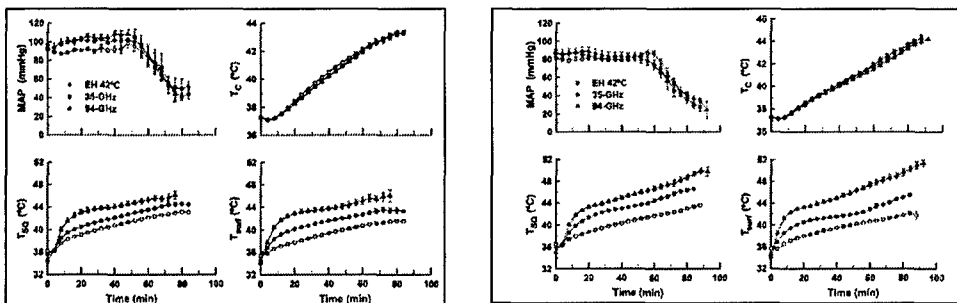
Figure 2: Comparison of ketamine and xylazine (left) with isoflurane (right) anesthesia. Upper left in each graph is mean arterial pressure; upper right is colonic temperature; lower left is subcutaneous temperature; and lower right is surface temperature. Three exposure conditions are explored: environmentally heated at 42°C; exposed at 35 GHz at 90 mW/cm²; and exposed at 94 GHz at 75 mW/cm².

The exposure conditions selected provided a method of matching the colonic temperature response of the environmentally heated, 35 GHz, and 94 GHz treated animals (upper left quadrant). Under these heating conditions the animals would typically go into irreversible shock shortly after 60 minutes of continuous exposure. Although the colonic temperature matched well under the three exposure conditions with both anesthetics, the 94 GHz exposed animals had higher subcutaneous and surface temperatures than either of the other two exposure treatments. As can be seen in figure 3, at the time of death for 35 GHz exposed animals the colonic temperature was nearly the same; however, the expiring time was nearly 30% longer, as well as the exposure time.
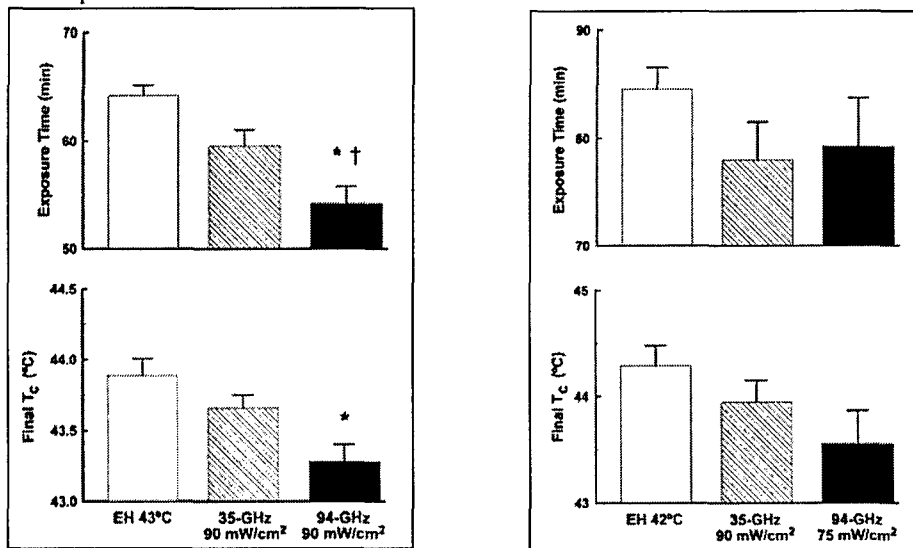
Figure 3: Comparison of method an anesthesia employed on time-to-death and final colonic temperature. Left graph provides data for ketamine and xylazine anesthetic and the right graph provides data for isoflurane anesthetic (taken from Millenbaugh et al. 2006). The 35 GHz exposure conditions were the same for both anesthetics employed; unlike the environmentally heated and 94 GHz exposures.

Animal maintenance:

Animals were maintained in a manner similar to that described in Millenbaugh et al. 2006. Male Sprague-Dawley rats (Charles River, Raleigh, NC) weighing 350-400 grams were housed individually in standard polycarbonate, solid-bottom cages with free access to water while access to food was carefully monitored to maintain size and weight. If a rat exceeded 400 grams, it was placed on a weight-restricted diet, normally 75% of what the rat would eat normally and held to between 350 and 400 grams. Water was provided *ad libitum*. The night before an exposure, the animal was denied chow. Room temperature was held from 22°C to 24°C and a 12:12 h light-dark cycle (lights on at 0600 h) was used. Experimental procedures were all performed from 0600 h to 1800 h and exposures from the different treatment groups were randomized. Animals were typically introduced into the protocol in groups of 40 and all animals were placed into exposure within two months of entering our care. Strict adherence to the National Institute of Health Guidelines on the Use of Laboratory Animals was maintained and experimental procedures were approved by the Institutional Animal Care and Use Committee of the Air Force Research Laboratory, Brooks City-Base, Texas and were conducted in compliance with the *Guide for the Care and Use of Laboratory Animals* prepared by the Committee on Care and Use of Laboratory Animals of the Institute of Laboratory Animal Resources-National Research Council and U.S. laws.

Exposure preparation and instrumentation

Rats were initially anesthetized with 4% isoflurane (Isosol; Vedco, St. Joseph) and were maintained under 2.5% isoflurane throughout exposure by means of a calibrated rodent anesthesia system (IMPC6; VetEquip, Pleasanton, CA). The left flank was shaved with electrical clippers revealing approximately 16% of skin surface extending from the dorsal midline to the ventral midline and thorax to pelvis. The right flank was not disturbed and was used as a control. These anesthetized animals were then placed on a Styrofoam platform lying on their ventral side with the shaved flank facing the MMW transmitter. A thermistor probe (BSD Medical Corporation, Salt Lake City, UT) was centered beneath the shaved flank to measure subcutaneous temperature and another was inserted 5 cm into the colon to measure colonic temperature. Both probes were secured with micropore tape on the tail. The posterior legs and the left anterior leg were taped onto the platform to prevent any movement during exposure. Surface temperature was measured with a Merlin™ infrared camera (FLIR systems, Indigo Operations, Goleta, CA) calibrated with an M340 black-body source (Mikron Instruments; Oakland, NJ). Temperatures from all three sites as well as the ambient temperature in the exposure chamber were recorded with LabView software (National Instruments; Austin, TX) on a Dell computer.

> **Comment [m1]:** Bob: Are you sure FLIR systems is part of Indigo Operations? They use to be separate companies?

Millimeter Wave Exposure

All animals were either cooled (passively) or heated (with heating pad) to a body core temperature of 37.3°C prior to exposure. Once this temperature was reached, temperature recording commenced with a three minute equilibration and then MMW exposure began. Rats were exposed on the left flank to 60 minutes of continuously applied 50, 75, or 100 mW/cm^2 at MMW in an Eccosorb RF-shielded anechoic chamber. A 50-Watt transmitter from Applied Electromagnetics, Inc. (Atlanta, GA) was used while a Varian VKB2462L2 gridded extended oscillator emitted at a frequency of 94 GHz. The incident power density of the field was determined at the exposure site with an isotropic probe in conjunction with an electromagnetic

survey meter (Models 8723 and 8718, Narda Microwave Co.; Hauppauge, NY). The ambient temperature of the exposure chamber was adjusted to either 23°C or 33°C depending on treatment.

Exposure parameters were such that the power density values decreased from a central area of approximately 1 cm in diameter (the "hot spot"). After exposure, the hot spot on the animal was identified with the last image recorded by an infrared (IR) camera and was marked with a black pen. The right flank was then shaved and an area similar to the one marked for the hot spot was also marked. Anesthetized rats that were maintained alive during exposure were sacrificed by CO_2 asphyxiation after the termination of exposure. The marked areas plus 4 to 6 cm of skin surrounding those areas were harvested immediately and fixed in 10% buffered formalin for 24 hours. From this rectangular section, two intersecting 3 cm pieces of tissue were cut forming an X with the hot spot at the center. This tissue was then processed and embedded in paraffin blocks through the short schedule method described by Prophet [1994]. All physiological data was arrayed and analyzed using Microsoft Excel™ spreadsheets.

Animals allowed to recover did not have subcutaneous probes attached to lessen chance of infection. Recovered animals were returned to the animal colony for an appropriate period of time with free access to food and water. When the specific recovery time was reached, the animals were sacrificed by CO_2 asphyxiation as described above.

Some 35 GHz exposures were made with the same power density criteria as the 94 GHz exposures. Much of the data obtained with 35 GHz exposures remains to be analyzed and only that work involving thermographs is reported here.

Image Processing and Data Collection

Blocks of tissue were chilled and sections 6 μm thick were cut and mounted on to glass slides. A general hematoxylin and eosin stain protocol was performed and digital images of prepared slides were collected using a Spot Insight™ 14.2 Color Mosaic digital camera (Diagnostic Instruments; Sterling Heights, MI) mounted to an Olympus (Central Valley, PA) CX31 light microscope.

Site Selection and Thresholding Measurements

Examination of exposed tissue lead to the observation that the most notable effect of prolonged 94 GHz exposure was the retraction of muscle fibers from the surrounding endomysium. Because of this, the amount of clear endomysial space in an area of muscle tissue was measured as an indicator of injury from prolonged 94 GHz exposure. Similarly, it was noted that there was an apparent decrease in interstitial spacing in the dermis of exposed rat skin. Background light was optimized and digital image thresholding was performed using the FoveaPro™ analysis software package (version 3; Reindeer Graphics, Inc., Asheville, NC) for Adobe Photoshop CS2™. Tissue samples were taken from the hot spot, the area of highest power density and thus temperature. Figure 4 provides a pictorial representation of tissue selection.
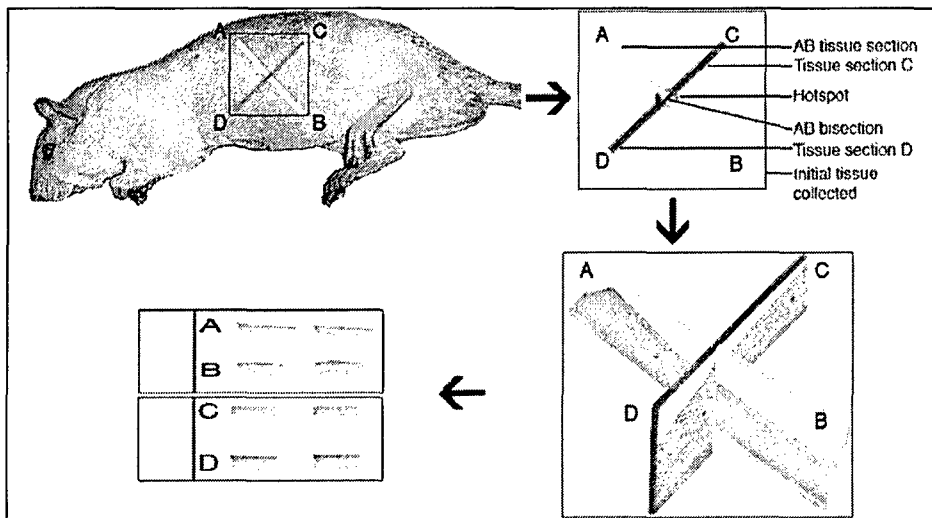
Figure 4: Method of tissue selection for microscopy. The area of highest final surface temperature is marked as the "hot spot." Pieces of skin tissue are taken as indicated with the hot spot located at the end of each tissue strip. Two consecutive sections are taken and mounted as shown.

Bands of adipocytes, variable distribution of hair follicles, and mechanical artifact from tissue preparation would make a whole tissue or tissue-layer image threshold inaccurate. Because of this inaccuracy in the dermis, approximately five rectangular areas without this variability were randomly selected from the hot spot area of each experimental animal. The number of rectangular areas per sample examined varied because of the presence of interruptions such as hair follicles that would skew data, but the total area examined was approximately equal. Panniculus carnosus muscle did not exhibit the same variables as dermis, however areas were also selected to avoid mechanical artifact. The number of white and black pixels from rectangular areas were summed and expressed as percentages. Tissue differences were quantified as white and black pixels, with white being representative of interstitium in the dermis or of clear endomysial space (CES) in the panniculus carnosus muscle.

Methodology associated with objective A.
Injury Score
An injury score was applied to each exposure based on the digital images obtained. Four categories of injury response (clear endomysial space, extravasation, blood vessel dilation, and blistering) were assigned a value from 0-3 with a maximum injury score of 12 possible. A value of 0 was assigned if there was no evidence of the response in the tissue sample; a value of 3 was assigned if the response was highly evident in the tissue. Values of 1 and 2 were reserved for intermediate response degrees. Tissue samples were examined in a single-blinded method.

Neither the animal nor exposure condition was revealed to the researcher assigning the injury scores to the tissue. Two researchers assigned injury scores to each sample and the two scores were averaged and used as the reported values of injury response.

Injury Threshold Calculations

The injury score data was combined with the temperature data in order to calculate the temperature threshold for each of the four specific injury responses to be observed in the tissues. A binary system was used in order to simplify the threshold calculations. A value of 0 or 1 for the injury score was considered unobserved and was assigned a value of 0 in the binary system. In addition, a value of 2 or 3 for the injury score was considered observed and was assigned a value of 1 in the binary system.

The maximum surface temperature was averaged with the maximum subcutaneous temperature reached for each exposure. This method was used because it is known that MMW exposure heats from the inside first, rather than the outside first as seen in typical thermal applications.

The averaged maximum surface and subcutaneous temperature was then graphed versus the binary injury data. Using this graph the threshold temperature was found by taking the four temperature values for the binary scores of 0 and for the binary scores of 1 nearest to the transition point where the values go from 0 to 1. These eight temperature values were then average in order to find the threshold temperature for each injury response. Student t-tests were performed on the temperature threshold in order to find if the threshold was significant.

Methodology associated with objective D:

A trial and error approach was employed to define the use of a heating pad under the anesthetized animal to maintain the colonic temperature at 37.3°C. This was accomplished with five timed applications of one minute each ("temp bumps") with the water-based heating system.

Methodology associated with objective F:

The left lateral flank was shaved from the dorsal to ventral midline and from the pectoral to pelvic girdle, revealing approximately 20% of the skin surface, to which a power density of either 75 mW/cm^2 (94 GHz) or 100 mW/cm^2 (35 GHz) was continuously applied. Exposure concluded when the core body temperature reached 41°C (averaging 52 min at 35 GHz and 82 min at 94 GHz). The purpose of this study was to correlate MMW influenced surface temperature to underlying skin histology. After euthanizing the animal, an approximate 12 by 8 cm piece of flank skin was removed and stapled to an index card to prevent shrinkage. The tissue was then fixed in 10% buffered formalin. This fixed skin was subdivided into 1 by 2 cm samples that corresponded to a similar grid overlying the thermograph. The skin tissue was paraffinized, sectioned at a thickness of 6μm, and stained with hematoxylin and eosin. Digital microscope images were analyzed from each corresponding grid sample for average dermis thickness, adipose thickness, and percentage of dermis area occupied by hair follicles. These data were correlated to the surface temperatures shown on the thermograph.

Results:

A) Relationship of Power Density to tissue response to 94 GHz

Animals were exposed to 94 GHz MMW at 50, 75, or 100 mW/cm^2 power density for 60 minutes during which surface, subcutaneous, and colonic temperatures were monitored.

Following exposure the animals were sacrificed and skin tissue was collected, processed histologically, and digital images of the tissue were obtained. The digital images and temperature data were combined to find the temperature threshold for four types of injury response (clear endomysial space increase, 42.1°C; blood vessel dilation, 42.9°C; extravasation, 42.9°C; blistering, 44.1°C) in response to MMW exposure.

Temperature Response

Average surface, subcutaneous, and colonic temperature recorded during exposure to 94 GHz MMW is shown over the length of exposure by power density in figure 5. From the graphs it can be observed that exposure to 100 mW/cm² caused the highest temperature increase in all three regions, exposure to 50 mW/cm² power density caused the least temperature increase in all regions, and exposure to 75 mW/cm² caused an intermediate temperature increase with values between the 50 and 100 mW/cm² exposures. Standard deviations were calculated for each power density, but are not shown in the graphs for simplicity. The standard deviation bars for any of the power densities did not overlap.

The surface temperature (figure 5A) and subcutaneous temperature (figure 5B) increased rapidly upon commencement of MMW exposure as indicated by the steep slope and rapid temperature rise seen within the first ten minutes of exposure. After the first ten minutes of exposure the surface and subcutaneous temperatures continued to increase, but at a slower rate of temperature increase. Colonic temperature response to the MMW exposures is shown in figure 5C. Unlike surface and subcutaneous temperatures, the colonic temperature is slower to respond to the heat and does not increase its temperature as rapidly as either the surface or subcutaneous regions. For the first 10 minutes of MMW exposure at all power densities there is essentially no change in the colonic temperature; however, after the first 10 minutes of MMW exposure the colonic temperature undergoes a linear increase in temperature. Lines were fit to the surface, subcutaneous, and colonic temperatures from 0-60 minutes exposure period and displayed in figure 16 (next section).

Figure 6 represents the same temperature data as figure 5, but arrayed by power density rather than region of temperature recording. The 50 mW/cm² exposure data is shown in graph A, the 75 mW/cm² exposure data is shown in graph B, and the 100 mW/cm² exposure is shown in graph C. By looking at the data arrayed in this manner it is evident that the extent of tissue heating is highly dependent on power density.

In response to the 50 mW/cm² exposures (figure 6A), the surface and colonic temperatures eventually follow the same temperature progression after the first 10 minutes of exposure. Additionally the subcutaneous temperature follows a similar temperature progression only slightly higher than the surface and colonic temperature progressions. In response to the 100 mW/cm² (figure 6C) the surface and subcutaneous temperatures follow essentially the same temperature progression, while the colonic is follows a much lower temperature progression. The 75 mW/cm² (figure 6B) exposure power, like the 100 mW/cm² exposures, has a surface and subcutaneous temperatures that follow similar temperature progressions, but unlike the 100 mW/cm² exposure level the surface and subcutaneous temperatures are only slightly higher than the colonic temperature. In addition, at the end of the 75 mW/cm² exposure the colonic temperature essentially reaches the same temperature level as the surface and subcutaneous temperatures.
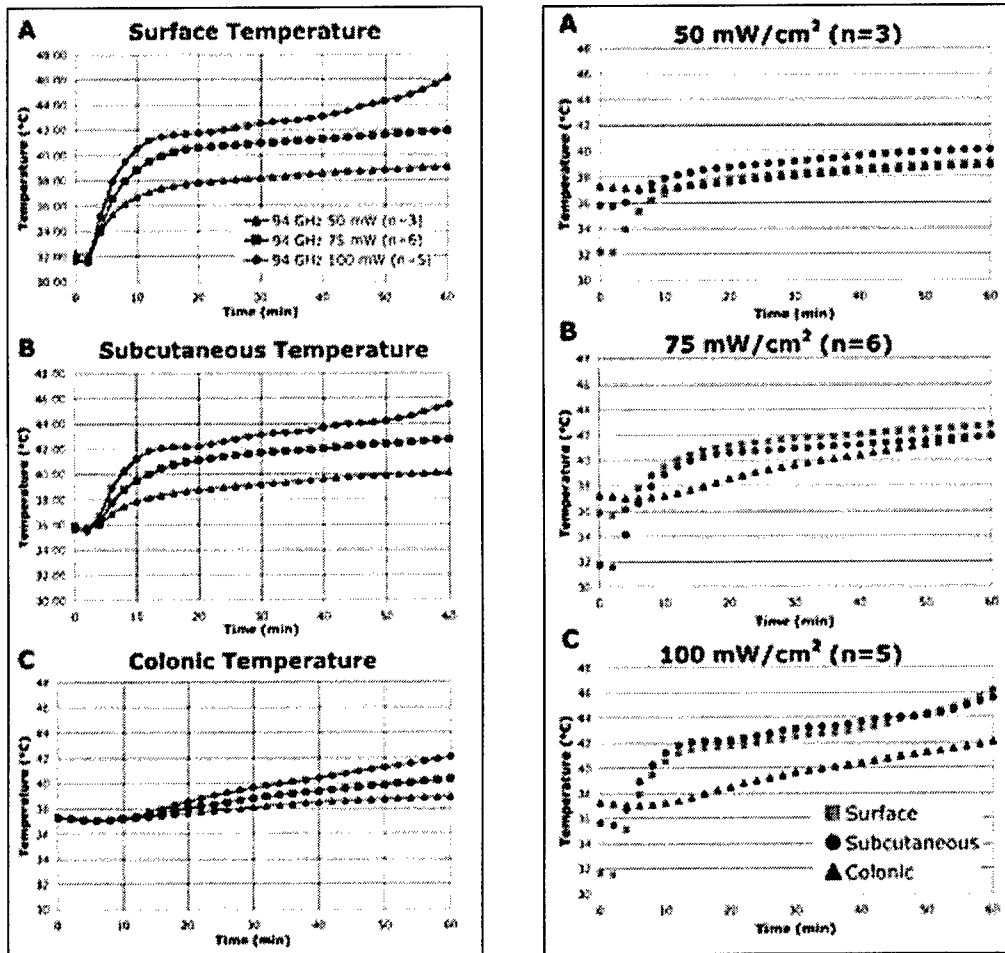
Figure 5 (left): Surface temperature response (**A**), subcutaneous temperature response (**B**), and colonic temperature response (**C**) were recorded over the sixty-minute exposure period. The higher power exposures are associated with higher temperature levels reached. When standard deviation was performed these sets of power densities were not within range of each other. The colonic temperatures in (**C**) show a linear relationship to the increases in power density.

Figure 6 (right): 50 mW/cm^2 temperature response (**A**), 75 mW/cm^2 response (**B**), and 100 mW/cm^2 response (**C**) were recorded over the sixty-minute exposure period. The temperature data used is the same as figure 5, but arrayed by power density rather than region of temperature recording. The 50 mW/cm^2 exposure shows the surface and colonic temperature values following the same heating pattern after the first 10 minutes of exposure. For the 75 and 100 mW/cm^2 exposure the surface and subcutaneous temperatures follow essentially the same heating pattern and have higher temperature values than the colonic temperature.

Histological Response

The response of the skin tissue to the MMW exposures was analyzed using histological techniques and digital imaging. Figures 7-10 show representative digital images of histological responses to 94 GHz MMW exposures at each power density levels. Animals were exposed on their left lateral flank and the exposed tissue was compared to their right unexposed tissues. For figures 7-10, panel A shows 50 mW/cm^2 exposed unresponsive tissue, panel B shows 75 mW/cm^2 exposed unresponsive tissue, panel D shows 75 mW/cm^2 exposed responsive tissue, and in panel C 100 mW/cm^2 exposed responsive tissue is shown.
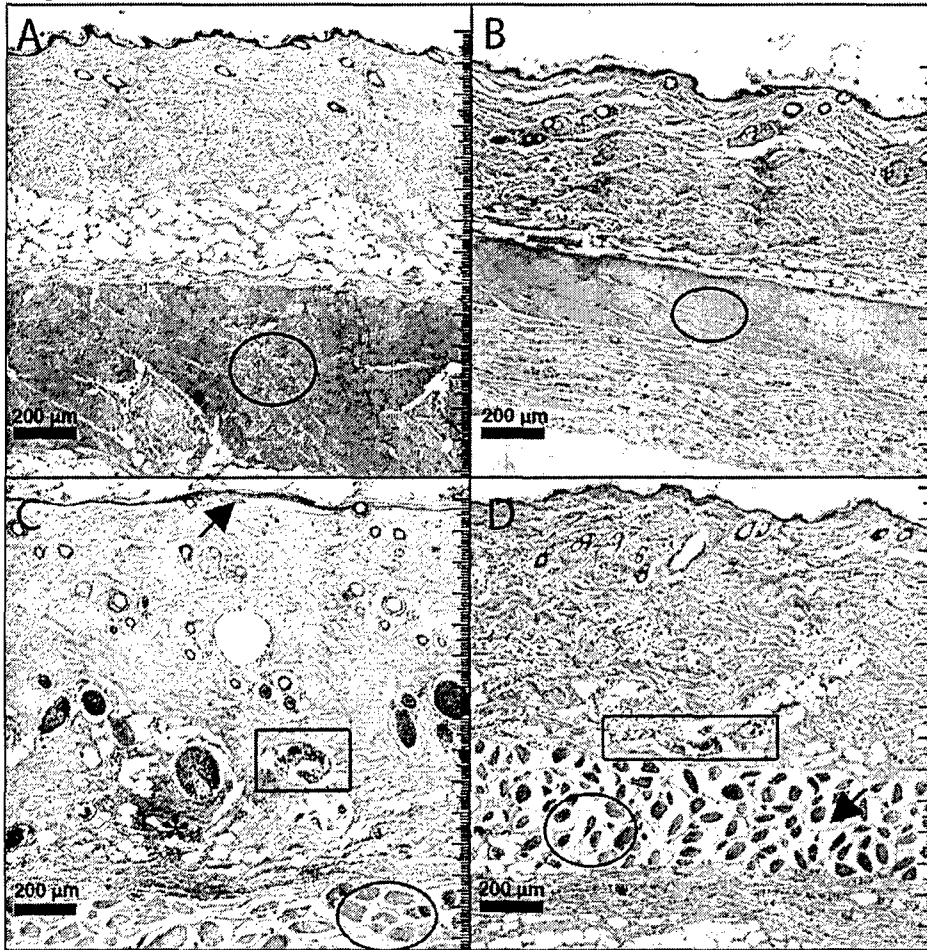
Figure 7: Comparison of rat skin tissue response to 94 GHz RFR at power densities of 50 (A), 75 (B and D), and 100 (C) mW/cm^2 for 60 minutes delivered at 23°C ambient. All images are at same magnification with bar scales on figure. A) Animal exposed to 50 mW/cm^2. The skin tissue appears normal, especially when compared to the unexposed contralateral right flank skin. B) Animal exposed to 75 mW/cm^2. The tissue is similar to panel A although this skin area displays less adipose tissue and the underlying muscle band is thinner and at a different angle of section. An example of a below threshold response. C) Animal exposed to 100 mW/cm^2. The dermis is swollen and the underlying paniculus carnosus muscle is quite disturbed. There is evidence of vasodilation in the reticular dermis. (Up arrow shows blistering, horizontal arrowhead shows dilated blood vessel, and down arrow shows muscle interstitial space) D) Animal exposed to 75 mW/cm^2. The paniculus muscle and vasodilation are similar to panel C. The reticular dermis is affected but not as profoundly as panel C. An example of an above threshold response. (Up arrow indicates dilated blood vessel, and down arrow indicates muscle interstitial space.
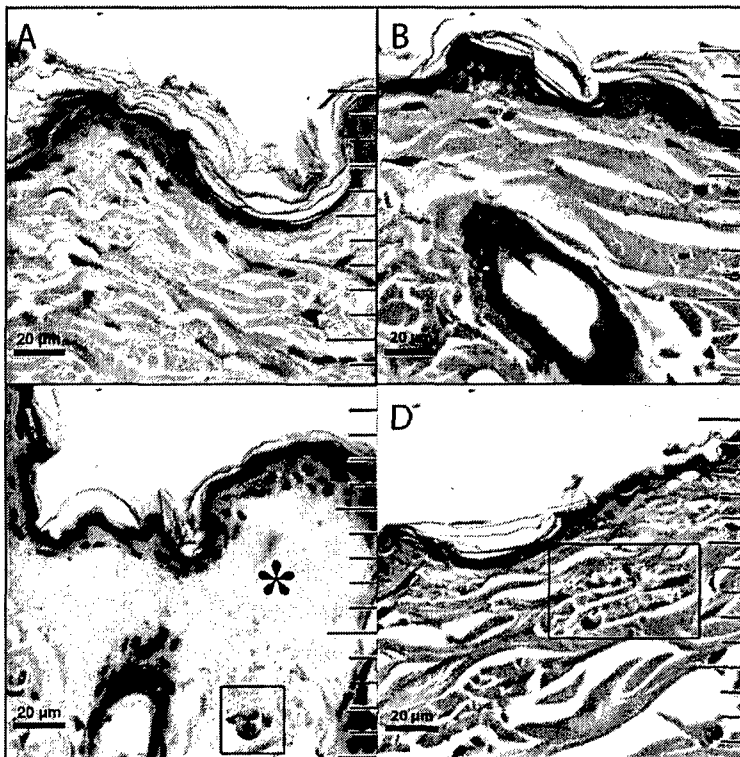

The right unexposed lateral flanks at each power density were found to compare favorably to control tissue at all power densities. No significant histological responses were observed in the unexposed right side tissue. It was found that the lowest power density level, 50 mW/cm^2, shown in panel A of figures 7-10 showed no histological response to the MMW exposure and compared favorably to its unexposed contralateral tissue. Thus the 50 mW/cm^2 tissue shown in panel A represents how tissue looks under normal conditions.

Figure 8: A ten-fold increase of magnification to reveal epithelium/papillary dermis of areas represented in Figure 1. Same panel orientation as figure 1: 50 (A), 75 (B and D), and 100 (C) mW/cm^2 power densities delivered at 94 GHz for 60 minutes and 23°C ambient. All images are at same magnification with bar scales on figure. A) Animal exposed to 50 mW/cm^2. The

epidermal layer is one cell thick and the nuclei of dermal fibrocytes (blue) compare well with control tissue. B) Animal exposed to 75 mW/cm^2. The tissue compares favorably with control and panel A. An example of a below threshold response. C) Animal exposed to 100 mW/cm^2. The epidermis is multilayered with early evidence of blistering (separation of the epidermis from the papillary dermis). Fibrocyte nuclei are contracted in contrast to some evidence of papillary capillary dilation. D) Animal exposed to 75 mW/cm^2. This tissue, which is above threshold response, demonstrates dilated capillaries and some condensation of fibrocyte nuclei.
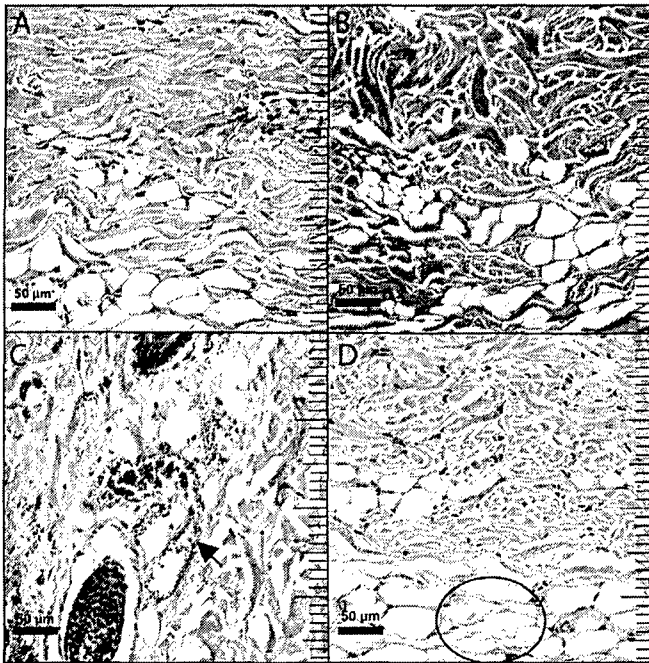
In contrast, the highest power density (100 mW/cm^2) shown in panel C of figures 7-10 shows considerable histological response as compared to both its unexposed tissue and the exposed 50 mW/cm^2 tissue. Between the two extremes a threshold of tissue response was found to occur at the 75 mW/cm^2 power level. Some of the animals exposed to the 75 mW/cm^2 power density showed histological response, while others exposed at the same power density showed no tissue response. The 75 mW/cm^2 tissue that was unresponsive (see panel B of figures 7-10) looked similar to the 50 mW/cm^2 exposures. The 75 mW/cm^2 exposures that showed tissue response (see panel D of figures 7-10) resembled the 100 mW/cm^2 exposures.

Figure 9: A four-fold increase of magnification to reveal reticular dermis near hypodermis of areas represented in Figure 1. Same panel orientation as figure 1: 50 (A), 75 (B and D), and 100 (C) mW/cm^2 power densities delivered at 94 GHz for 60 minutes and 23°C ambient. All images at same magnification with bar scales on figure. A) Animal exposed to 50 mW/cm^2. The reticular dermis compares well with control tissue. B) Animal exposed to 75 mW/cm^2. The tissue compares favorably with control and panel A. An example of a below threshold response. C) Animal exposed to 100 mW/cm^2. The interstitium between dermal collagen is very limited suggesting swelling. Capillary dilation is very pronounced. The epidermis around hair follicles is indistinct. Various types of nuclei appear condensed. D) Animal exposed to 75 mW/cm^2. This tissue, which is above threshold response, demonstrates irregular adipocyte margins. The dermal interstitium is very evident.

Figure 7 shows overview images obtained at 100X magnification of skin tissue response to the three power density levels of MMW exposures. Panels A and B show no tissue response to the MMW exposures, while in panels C and D there is significant tissue response to the MMW exposure. The most obvious tissue change is observed in the panniculus carnsosous muscle identified within the circles in the images. In the muscle that responded to MMW at the higher power densities, the fibers are retracted from the supporting endomysium. An increased white area between muscle fibers is visible and termed clear endomysial space (CES). The CES is indicated by an arrow in panel D and can also be seen within the circled areas of panels C and D. The panniculus carnosous muscle response to MMW exposure at the higher power densities is also seen at higher magnification (400X) in figure 10C and D.

Several other responses are visually evident in the images in figure 7. Among these responses includes blood vessel dilation that is indicated by a square in panels C and D. Additionally in panel C extravasation is evident and indicated by an asterisk. Blood vessel dilation and extravasation can also be seen at a higher magnification in figures 9 and 10. Figure 10 also shows dilated capillaries indicated by a square in panels C and D and a blister indicated by an asterisk in panel C.
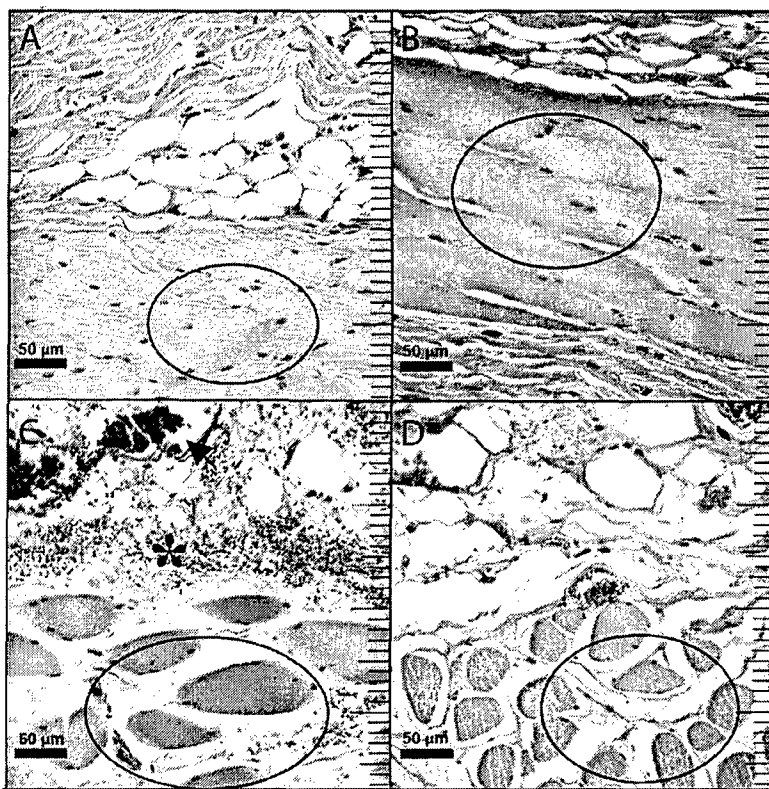
Figure 10: A four-fold increase of magnification to reveal the paniculus carnosus muscle areas represented in figure 7. Same panel orientation as figure 7: 50 (A), 75 (B and D), and 100 (C) mW/cm^2 power densities delivered at 94 GHz for 60 minutes and 23°C ambient. All images at same magnification with bar scales on figure. A) Animal exposed to 50 mW/cm^2. The obliquely sectioned paniculus carnosus muscle appears normal. B) Animal exposed to 75 mW/cm^2. The longitudinally section paniculus carnosus muscle compares favorably with control and panel A, although stained darker. An example of a below threshold response. C) Animal exposed to 100

mW/cm^2. The interstitium around individual necrotic muscle fibers is extremely swollen. There a profound lesion evident. D) Animal exposed to 75 mW/cm^2. Similar to panel C, the interstitium around muscle cells is evident. The lesion at this time is not quite as profound as panel C. The nearby adipocytes are disturbed.

Quantification of Interstitial Space

In order to quantify CES response to 94 GHz MMW, a thresholding analysis was performed using Fovea Pro™ for Photoshop™ and is shown in graphical form in figure 11C. The 100 mW/cm^2 exposure level shown in panel C in figures 7 and 10 was found to increase clear endothelial space significantly (p<0.05; see figure 11C) as compared to its unexposed right side tissue and as compared to the 50 mW/cm^2 exposures. In addition several of the 75 mW/cm^2 exposures also showed significant increases in clear endomysial space. However, unlike the 100 mW/cm^2 exposures not all of the 75 mW/cm^2 had an increase in clear endomysial space.

In addition to using thresholding analysis via Fovea Pro™ to find the percentage of CES thresholding was also performed on the dermis interstitial space. Quantification of the percentage of dermis interstitial space as compared to the collagen fibers is shown graphically in figure 11B. Although the results are not significant a trend does present itself. It seems that upon exposure the dermis interstitial space increases as compared to unexposed tissue. Figure 11A shows the thickness of the skin as measured from the epidermis to the panniculus carnosus muscle. It was found that there is no trend in the thickness of the skin in response to MMW exposure.
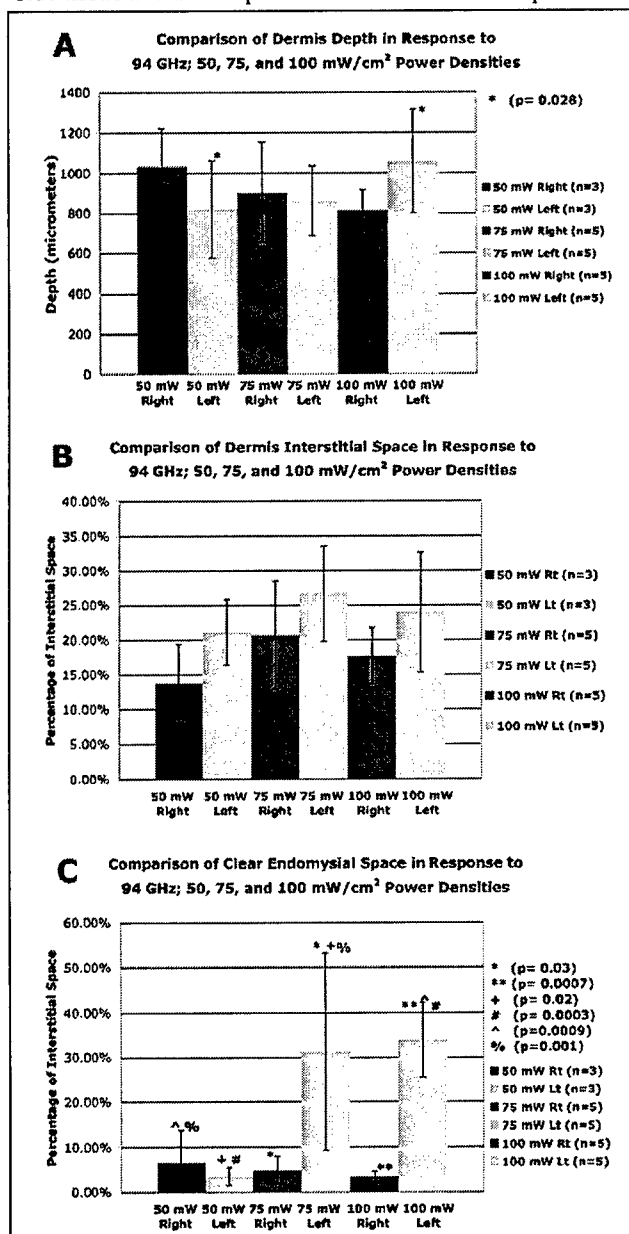
Figure 11: Shows dermis depth measurements in response to exposure (A), dermis interstitial space thresholding data (B), and clear endomysial space thresholding data (C). The dermis depth is highly variable with no

consistent trend likely due to variation in the hair cycle at the time of exposure. Although not significant, the dermis interstitial space has consistently higher values after exposure as compared to unexposed tissue. The clear endomysial space is significantly increased for both the 75 and 100 mW/cm^2 exposed tissue as compared to unexposed tissue and the lowest power density 50 mW/cm^2.

Injury Score

Figure 12 shows a graded score for each exposure assigned based on the injury responses observed in the digital images. Four criteria (muscle interstitial space, blood vessel dilation, extravasation, and blistering) were assigned a value from 0-3 for each exposure. A 0 score was ascribed if the injury was not observed while a score of 3 was assigned if the injury was very evident. Scores of 1 and 2 were reserved for intermediate responses observed.
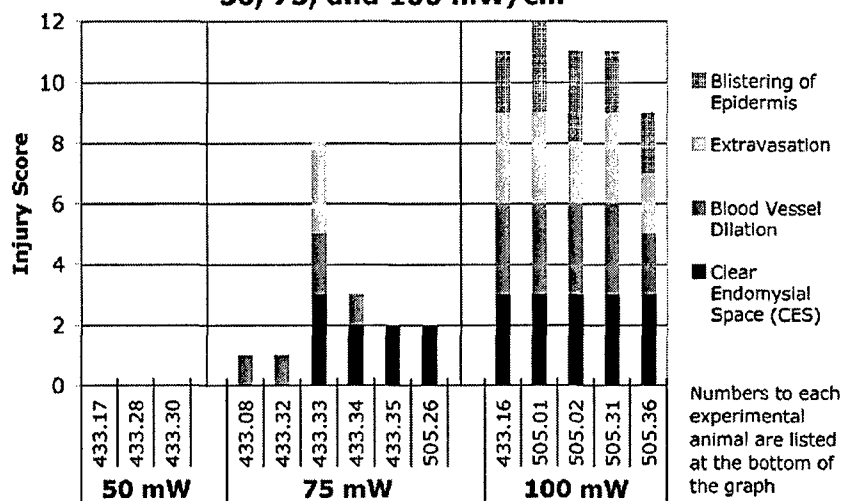
The graph shown in figure 12 clearly shows that no injury response is observed at the lowest power density level of 50 mW/cm^2. In addition, the graph suggests that the 100 mW/cm^2 exposures cause significant injury response as compared to the 50 mW/cm^2. It was also found that the 75 mW/cm^2 had intermediate injury responses to the MMW exposure.
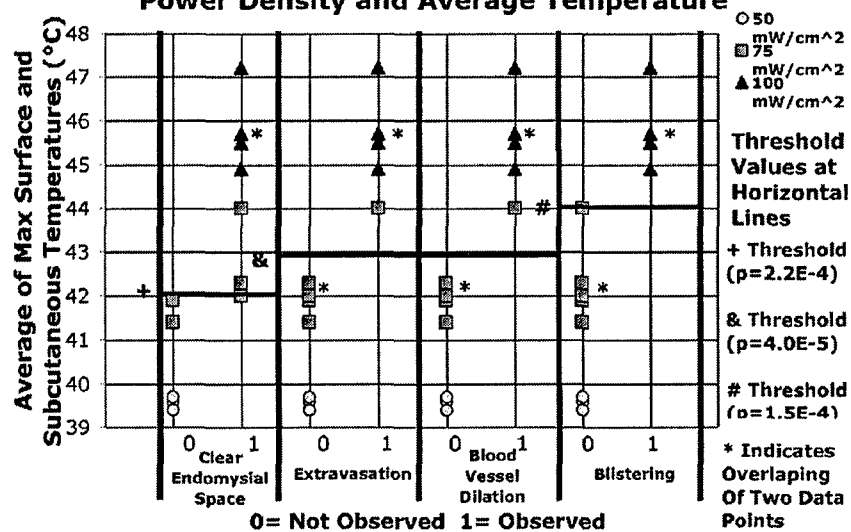
Temperature Injury Threshold

Combining data from figures 5 and 12 a binary system was used in order to calculate the threshold temperature for injury response (see figure 13). A value of 0 was used in figure 13 for injury responses that received a value of 0 for the injury score in figure 12. In addition in figure 13, a value of 1 was assigned for the injuries that received a score of 1,2, or 3 in the injury score graph of figure 12. A value of 0 in figure 13 was considered unobserved in response to the MMW exposure, while a value of 1 in figure 13 was considered observed in response to the MMW exposure. The binary system was used to analyze the effects of different power densities on four tissue responses (muscle interstitial space, extravasation, blood vessel dilation, and blistering).

Injury Scores in Response to 94 GHz Exposure
50, 75, and 100 mW/cm²

Legend:
- Blistering of Epidermis
- Extravasation
- Blood Vessel Dilation
- Clear Endomysial Space (CES)

Numbers to each experimental animal are listed at the bottom of the graph

Comparison of Tissue Injuries at 94 GHz to Power Density and Average Temperature

- ○ 50 mW/cm^2
- ▦ 75 mW/cm^2
- ▲ 100 mW/cm^2

Threshold Values at Horizontal Lines

+ Threshold (p=2.2E-4)

& Threshold (p=4.0E-5)

Threshold (p=1.5E-4)

* Indicates Overlaping Of Two Data Points

0= Not Observed   1= Observed

Figure 12 (on top): Shows the injury responses observed at each power density; 50, 75, 100 mW/cm^2 at 94 GHz. Injury responses were recorded as a value from 0-3 with 0 as not evident and 3 being highly evident. The 50 mW/cm^2 animals show in effect no response to the exposure. At the 75 mW/cm^2 power level significant injury was observed for some of the animals, while some of the animals at this same power density failed to respond suggesting a possible threshold level of injury response. The most obvious response seen at this level is the increase in the amount of muscle interstitial space. The 100 mW/cm^2 exposures all showed significant injury and is the only power level in which blistering is observed.

Figure 13 (on bottom): Shows tissue injury responses observed versus the average of the surface and subcutaneous temperatures and power density level. If injury responses were recorded as a minimum of 2 in graph A, then it was considered observed and assigned a 1 in this graph, if not then it was listed as a 0 in this graph. The graph shows three threshold levels indicated by the horizontal lines. These threshold levels consistently occur in the middle of the 75 mW/cm^2 exposures, but correspond to three different temperature levels of threshold. Blood elements including extravasation and dilation shared their threshold level. The p-values corresponding to each threshold level suggests that they are highly significant.

As discussed earlier the surface and subcutaneous temperatures respond similarly to the MMW exposure. In addition, it is known the MMW exposures heat beginning within the dermis rather than from the surface of the skin inward as would occur in a contact burn. Since the surface and subcutaneous temperatures obtained do not directly represent the temperature at the hot spot an average of the maximum surface and maximum subcutaneous temperatures for each exposure were computed. This data was then coupled to the injury scores as described in the methods section in order to obtain figure 13.

Using the data shown in figure 13, a temperature threshold level was identified for the clear endomysial space response, the blood elements (vessel dilation and extravasation having the same threshold level), and blistering. Two of the three threshold levels (muscle space and blood elements) fall within the 75 mW/cm^2 exposures ranges, while the blistering threshold falls just above the 75 mW/cm^2 exposures and just below the 100 mW/cm^2 exposures. CES response threshold was found to have a value of 42.1°C average maximum surface and subcutaneous temperatures. The vascular elements, both vessel dilation and extravasation, were found to have a temperature threshold of 42.9°C average surface and subcutaneous temperature. Blistering was found to occur only at the highest power density (100 mW/cm^2), and was found to have a threshold value of 44.1°C average surface and subcutaneous temperature.

## B) Exposure time variation and recovery time variation to 94 GHz
Duration of exposure
Histology
The histology of animals exposed to 75 mW/cm^2 displayed varying responses to different lengths of exposure. Fifteen-minute and 30-minute exposures (figure 14A and B) resulted in skin tissue with no apparent histological changes. Tissue exposed for forty-five minutes displayed changes in the collagen fibers in the reticular dermis with less interstitial white space

than 15 and 30-minute duration exposures (figure 14C). Approximately 2/3 of the animals exposed for 60 minutes displayed significant injury similar to that observed in animals exposed to 100 mW/cm^2 for 30 minutes. As shown in figure 14D, the muscle fibers pulled away from the endomysium resulting in large amounts of clear space around the fibers. The dermis also appeared inflamed and there was also evidence of dilated blood vessels and extravasation in the deep dermis. The remaining third of the animals treated at 75 mW/cm^2 demonstrated none of these changes.

Tissue exposed to a power density of 100mW/cm^2 clearly illustrated a progression of injury (figure 15). As the exposure period was increased, the associated histological changes of the skin escalated. The skin exposed for fifteen minutes showed no significant change (figure
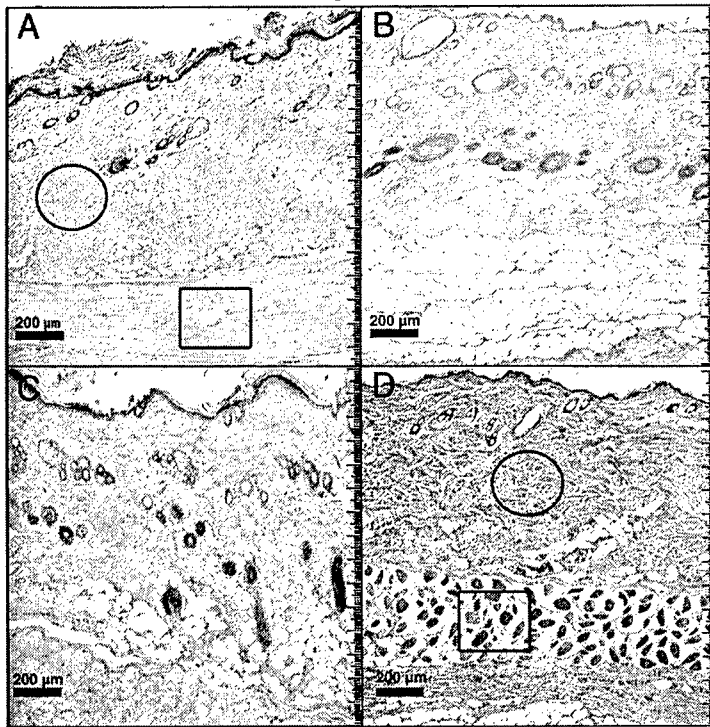
15A). The underlying muscle band did, however, display some retraction from the endomysium and separation of the muscle fibers. Thus, a histological response by muscle tissue was observed with as little as fifteen minutes exposure and injury escalated with increasing exposure length. At thirty minutes (figure 15B), vasodilation was evident in the dermis as well as extravasation in the deep dermis. The muscle fibers appeared contracted from the endomysium, creating large clear endomysial spaces (CES). Tissue exposed for forty-five minutes (figure 15C) displayed histological changes similar to that of tissue exposed for thirty minutes. However, large blisters under the epidermis were now evident. Skin exposed for sixty minutes displayed significant histological change from normal. The collagen in the dermis was no longer irregular with slight interstitial white space separation, but appeared to have fused together as if "melted". Blistering (not shown) was still evident. The hair follicles may also be showing some injury indicated by the white space between them and the surrounding collagen (figure 15D). This event was called the "halo effect.

Figure 14: Histology of rat skin exposed to four time intervals of 94 GHz MMW, 75 mW/cm^2, 23°C ambient. A) 15-minute exposure. The skin appears orderly and normal (circled area shows dermal collagen and boxed area shows muscle fibers). B) 30-minute exposure. The skin

appears orderly and normal. C) 45-minute exposure. The collagen bundle diameter is greater and the dermal interstitium between bundles is reduced. D) 60-minute exposure. The collagen bundle diameter (circled area=collagen bundles) is greater than in exposures at 15 and 30 minutes (compare to circled area Panel A). Limited vasodilation is evident at the dermal/muscle junction. The panniculus carnosus muscle fibers are highly condensed (boxed area).

Temperature data

Figure 16 provides the temperature data obtained during exposure as measured on the skin surface, subcutaneous (1 to 2 mm from the surface) and colonic (body core) regions. Liner regression curves suggest that for the first 15 minutes of exposure both the surface and subcutaneous temperatures are 2°C warmer at 100 mW/cm^2 power density. The endpoint for the body core for the same time interval is essentially identical at 38°C for both power densities. Table 2 provides per minute slope data for each 15-minute interval at both power densities. In every case, the per minute rate change is higher for 100 mW/cm^2. Especially interesting were the large differences between the two power densities at the surface and subcutaneous sites during the last 15-minute interval (45-60 minutes).

Table 3 expresses the Table 2 data as ratios with reference to body core temperatures. Differences in thermoregulation are suggested first by the elevated surface ratio during the third 15-

minute interval and in both the surface and subcutaneous sites during the fourth 15-minute exposure period for 100mW/cm^2. These different and accelerated temperature changes in rat skin are reflected in histological changes seen in figures 14 and 15.
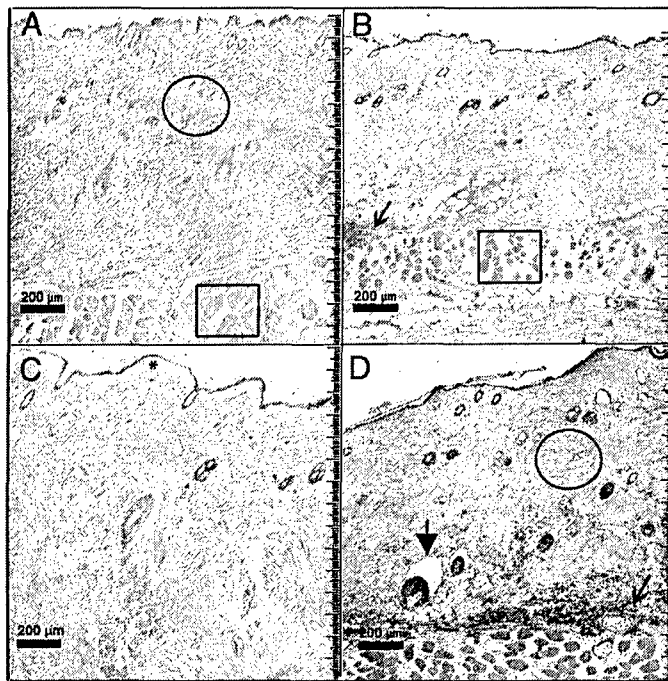
Figure 15: Histology of rat skin exposed to four time intervals of 94 GHz MMW, 100 mW/cm^2, 23°C ambient. A) 15 minute exposure. The reticular dermis (circled area) appears slightly coarser than the corresponding 75 mW/cm^2 exposure (See figure 14A). The panniculus carnosus muscle fibers (boxed area) exhibit some condensation. B) 30 minute exposure. This tissue is highly damaged. Extravasation at the adipose level is common (arrow). The myocytes are extremely condensed (boxed area). C) 45 minute exposure. Skin section was selected to represent the epidermal blistering seen at the

papillary dermis/epidermis interface (see asterisk). The muscle damage (not in view) is similar to panel B. D) 60 minute exposure. Dermal collagen bundles are quite swollen and the dermal interstitium reduced (circled area). Extravasation in the lower reticular dermis is extreme (thin arrow). Vasodilation is common. The panniculus carnomuscle is condensed. The thick arrow indicates when a follicle has separated from the dermis (follicular halo).

Table 2 The rate of temperature change (slopes) for 15 minute Intervals obtained from figures 16 and 17.

	0-15 min Period		15-30 min Period		30-45 min Period		45-60 min Period	
Surface: Slope	0.537†	0.598†	0.039*	0.070*	0.033*	0.087*	0.032*	0.161*
Subcutaneous: Slope	0.355*	0.444†	0.061*	0.079*	0.041*	0.061*	0.032*	0.113*
Colonic: Slope	0.045†	0.068†	0.080*	0.115*	0.051*	0.081*	0.047*	0.080*

75 mW/cm^2= white background, 100 mW/cm^2=grey background
* R^2 >0.9, † 0.9 >R^2>0.75

Table 3 Magnitude of temperature change in surface and subcutaneous tissue in relation to colonic ΔT in animals exposed at 75 mW/cm^2 (n=6, white background) and 100 mW/cm^2 (n=5, grey background)

| Time (min)	$\dfrac{\text{Surface } \Delta T}{\text{Colonic } \Delta T}$		$\dfrac{\text{Subcutaneous } \Delta T}{\text{Colonic } \Delta T}$	
0-15	12	8.8	8	6.5
15-30	0.5	0.6	0.8	0.7
30-45	0.6	1.1	0.8	0.8
45-60	0.7	2.0	0.7	1.4

Table 4 Temperature values of tissue at fifteen-minute intervals of exposure to 75 mW/cm^2 (n=6, white background) or 100 mW/cm^2 (n=5, grey background). Bold values represent values were histological insult was observed.

Time (min)	Surface (°C)		Subcutaneous (°C)		Colonic (°C)	
15	40.4	**41.6**	40.8	**42.2**	37.7	**38.1**
30	41.0	**42.7**	41.7	**43.3**	38.9	**39.9**

| 45 | 41.5 | 43.9 | 42.3 | 44.1 | 39.7 | 41.0 |
| 60 | 42.0 | 46.1 | 42.8 | 45.5 | 40.4 | 42.1 |

Table 4 contrasts the surface, subcutaneous, and colonic temperatures at the end of each 15-minute exposure period for both employed power densities. All animals exposed to 75 mW/cm2 at 23°C ambient survived the 60 minute application of 94 GHz. In sharp contrast the animals exposed to 100 mW/cm2 at 23°C expired at 59.2 ± 1.1 min into the exposure with demonstrable skin injury. The representative images in figures 14 and 15 suggest that panniculus carnsosus muscle injury, followed by dermal and vasculature changes, and concluding with epidermal blistering appear sequentially during the exposure period. See previous section for sequencing of injury in greater detail at these exposure levels.

The rate of temperature change data seen in figure 17 demonstrates that the heat rise is maximal at the skin surface at 2 minutes into the exposure, maximal in the subcutaneous area at 4 minutes into the exposure, and maximal in the colonic area at 18 minutes into the exposure. There is progression of heat into the body and a progression of injury associated with that heat movement.
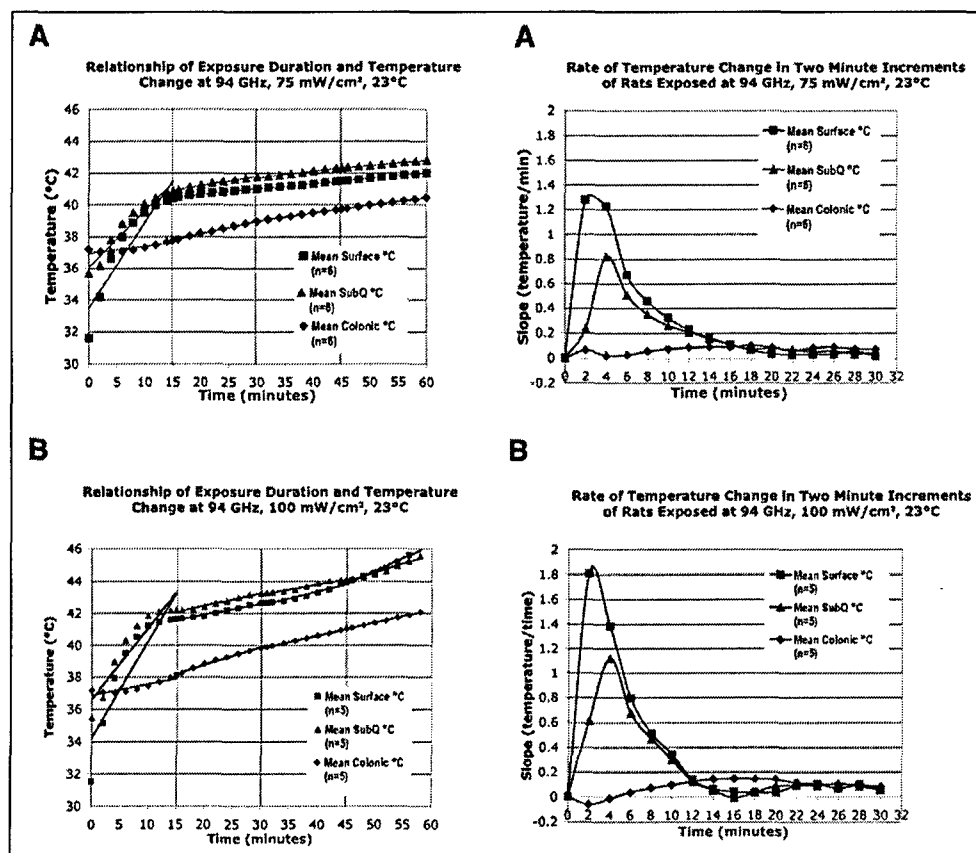
Figure 16 (on left): The graphs demonstrate the relationship between exposure duration and temperature change at 94 GHz a) 75 mW/cm^2 and b) 100 mw/cm^2, 23°C for four 15-minute intervals. The slopes of the lines denote the rate of temperature change in each fifteen-minute interval. See Table 2 for values.

Figure 17 (on right): The rate of temperature change calculated in two minute increments in living animals exposed at 94 GHz a) 75 mW/cm^2 and b) 100 mW/cm^2 at an ambient temperature of 23°C. Panel A illustrates that the surface temperature increased dramatically with the onset of MMW exposure and reached its peak at two minutes. Subcutaneous temperature trailed behind, reaching its peak at four minutes into the exposure. The rate of change in colonic temperature peaked at about eighteen minutes. Panel B illustrate that rates of temperature change were higher at 100 mW/cm^2 exposures than the rates of temperature change in animals exposed to 75 mW/cm^2. Surface temperature increased immediately and reached its peak at three minutes. Subcutaneous temperature response to MMW peaks at four minutes and then decreases along

rate of surface temperature change. Rate of change in colonic temperature began increasing six minutes into the exposure and peaked at about eighteen minutes, similar to panel A.

Post-Exposure
Histology

As previously reported above (figure 14D), two-thirds of the animals exposed for 60 minutes at a power density of 75 mW/cm^2 and immediately sacrificed (zero-day post-exposure) demonstrated above injury threshold responses. A distinguishing feature of their injuries was termed "dermal melt": the dermal interstitium was reduced and the collagen lost its distinctiveness. This "melt" phenomenon carried over into post-recovery animals and was used to separate these animals into two groups: "A" responders (above injury threshold) and "B" responders (below injury threshold). All animals exposed to 75 mW/cm^2 demonstrated histological changes in the post-exposure follow-up.
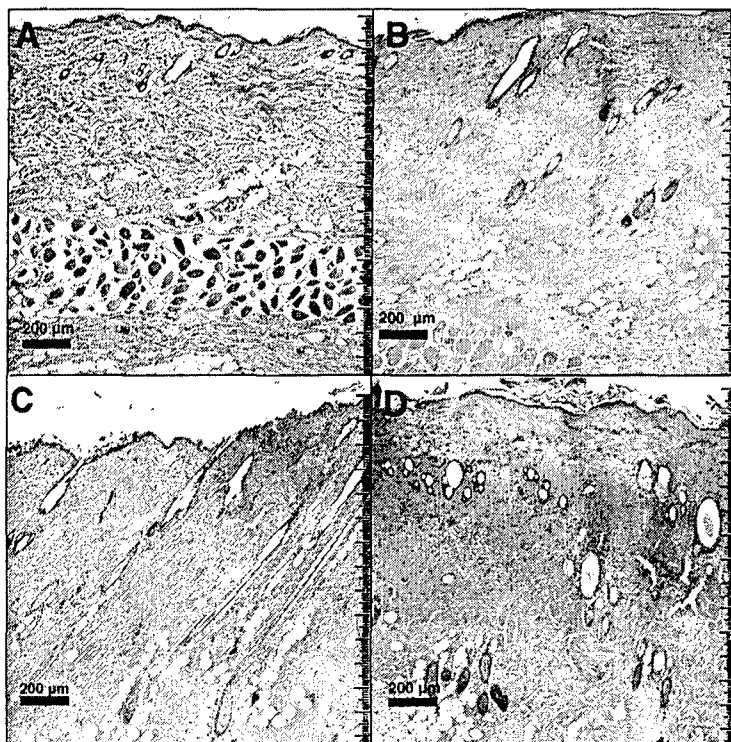
The A responders showed progressive changes in histology each successive day of post-exposure. Although no leukocytes were evident immediately after exposure (figure 18A), on subsequent days leukocytes were present in the injured dermis and muscle. One-day post-exposure animals (figure 18B) had affected epidermis and the "melt" was visible throughout the dermis. The underlying panniculus carnosus muscle no longer demonstrated its striation pattern. The B responders at one-day post-exposure, without dermal melt, did have disturbed collagen fibers, blood vessel dilation, and leukocytes in the deep dermis.
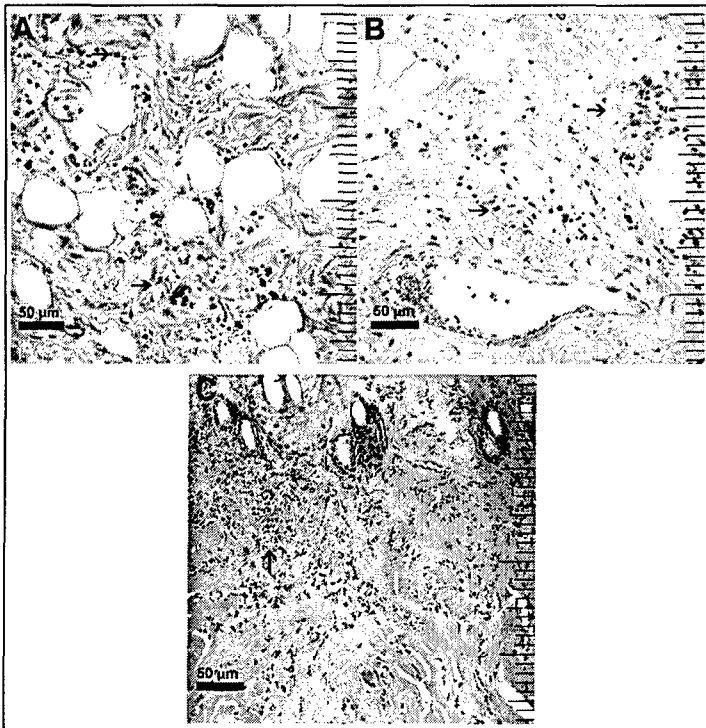

Figure 18: Comparison of rat tissue response to 94 GHz MMW at power density of 75 mW/cm^2 for 60 minutes delivered at 23°C ambient. All images are at the same magnification with bar scales on figure. A) Skin tissue collected immediately after exposure (i.e. Zero day post-

exposure). Notable are disturbed dermis collagen fibers and vasodilation in the reticular dermis. The underlying panniculus carnosus muscle layer is heavily injured. B) Skin tissue collected one-day post-exposure. Tissue shows necrosis of the papillary dermis and a disturbed reticular dermis that has assumed a "melted" appearance. Also observed is the fused appearance of panniculus carnosus muscle fibers. C) Skin tissue collected two days post-exposure. Similar to tissue shown in panel B, necrotic tissue is evident in the upper left portion of the image along with infiltration of leukocytes. The reticular dermis appears swollen. Some dermal collagen appears dense and "melted" (e.g. upper left corner and in the deep dermis). D) Skin tissue collected three days post-exposure. The tissue appears similar to that of panel C, but the papillary and reticular dermis are more profoundly injured ("melted"). Also observed is evidence of leukocyte infiltration in the middle area of the dermis.

Two-day post-exposure animals provided evidence of the greatest tissue injury in both A and B responders. At the extreme no dermal interstitial white space was evident, the dermis was contracted, and epidermis was no longer intact. Blood vessel dilation was maximal and muscle fibers had no continuity. Figure 18C provides a view of a B responder with less injury. The dermal collagen was disturbed and the papillary dermis appears necrotic with leukocyte invasion in full force. The epidermis is thinned. The reticular dermis is swollen and the panniculus muscle layer (not in view) has an infiltration of leukocytes among the denatured muscle fibers. The B responder tissue was demonstrating an inflammatory response at the histological level.

The A responders in three-day post-exposure animals (figure 18D) demonstrated necrosis of the epidermis and papillary dermis, similarly to injury seen in one and two-day post-exposure animals. An infiltration of leukocytes was apparent in the middle region of the reticular dermis and in the muscle layer. The B responder tissue displayed a similar response as the B responders in one-day post-exposure tissue. However, the tissue had many leukocytes in the deep dermis. (See also figure 19).

Figure 19: Leukocyte infiltration in skin 1, 2, and 3-days post-exposure to 94 GHz MMW at power density of 75 mW/cm^2 for 60 minutes delivered at 23°C ambient. All images are at the same magnification with bar scales on figure. A) Reticular dermis of skin one-day post-exposure. Many leukocytes and mast cells are clearly shown between denatured collagen fibers (arrows). B) Reticular dermis of

skin two-days post-exposure. Leukocytes are clearly evident in the injured dermis. The blood vessel in view seems dilated. C) Reticular dermis of skin three days post-exposure. Leukocyte infiltration in the necrotic tissue is more pronounced (arrow).

Tissue analysis and thresholding

Three histological responses of post-exposure animals were explored in greater detail: change in dermal interstitial space (white space), change in muscle clear endomysial space (CES), and change in dermis depth (thickness) (See figure 20). If the amount of white space in exposed tissue denotes the amount of injury, we hoped that quantifiable differences from the left (exposed) and right (not exposed) sides might be detected.

Figure 20A demonstrates that as the dermal interstitial space in exposed animals decreased over time, the unexposed right side interstitial space increased. The dermal interstitium responds inversely between exposed and unexposed skins. Exposed skin interstitium started high at 27% white space and then decreased to a value of 17.3% in three-day post-exposure tissue. In contrast, right side interstitial white space increased with increasing time allotted for recovery and reached a maximum in two-day post-exposure tissue (30%, data not shown). The interstitial white space subsequently decreased to a value of 23% three days post-exposure. The amount of white space in left side skin one-day post-exposure was statistically higher than in zero day or than in three-day post-exposure skin.
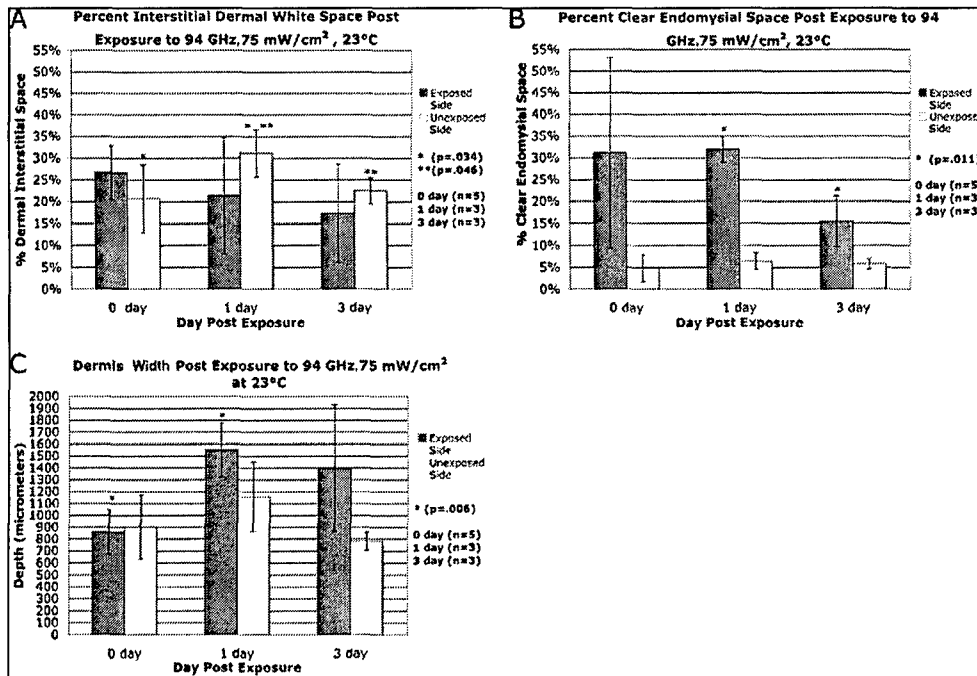

Figure 20: Histology analysis of 1, 2, and 3-day post-exposure skin (94 GHz, 75 mW/cm^2 MMW, 23°C ambient, 60 minutes) and unexposed skin. The percent dermal interstitium (panel

A), percent clear endomysial space in the panniculus carnosum (panel B), and the dermis thickness (panel C) were evaluated for three post-exposure time points (0, 1, and 3 days). T-tests were performed to determine significant differences.
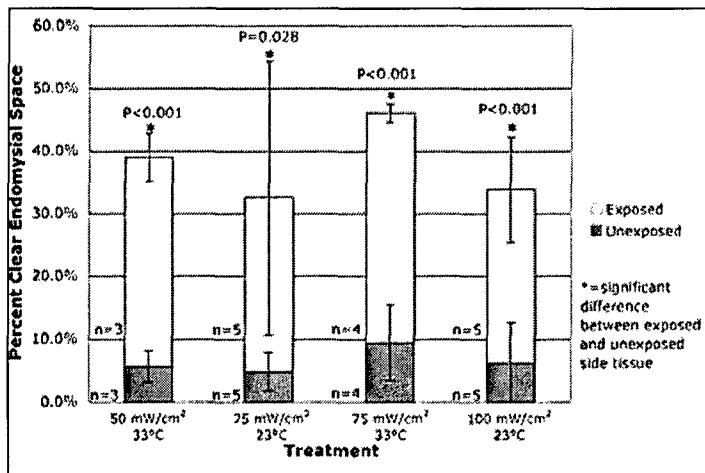
The CES in the panniculus carnosus muscle of exposed animals decreased with subsequent day post-exposure (figure 20B). Zero day and one-day post-exposure CES values of 31.2 and 31.9% respectively, showed that very little change in CES occurs in the first 24 hours. The large error bars in the values for zero-day and three-day post exposure tissue may be a factor of the variability observed in the level of tissue response, where some animals in a treatment displayed histological injury while others looked "normal". The results for the exposed tissue suggest that most muscle injury occurs immediately after exposure followed by one-day post-exposure. At two and three-days post-exposure, the tissue displayed less CES (14.9% and 15.5% respectively). The value for CES three-day post-exposure is statistically lower than the value for one day. Unlike the pattern of CES in the left side tissue, amount of muscle CES on the right side stayed fairly low and consistent.

Figure 20C illustrates that the dermis width of exposed tissue increased with increasing day post-exposure. The dermis width of zero-day post-exposure tissue (860 µm) was statistically lower than the width of one-day post-exposure tissue (1548 µm), which is about two times greater. The dermis thickness observed in two and three-day post-exposure tissue (1734 and 1395 µm respectively) was similar to the thickness observed for one-day tissue. The values are not statistically different. The dermis width values of unexposed right side skin followed a similar pattern as the values for the left side skin. The dermis width initially increased and then slightly decreased with recovery time. The differences observed in the unexposed side were not statistically significant.

C) The effect of ambient temperature on exposure response
Effects of MMW Exposure

Figure 21 displays the comparison of unexposed (right side) and 94 GHz exposed (left side) panniculus carnosus muscle CES after treatment with various power densities for approximately one hour or until death at either 23°C or 33°C ambient. There was no observed significant difference between exposed and unexposed side tissue for animals treated with 94 GHz delivered at 50 mW/cm^2 at an ambient temperature of 23°C (n=3 for both treated and untreated animals, p=0.26). Each of the other indicated treatments (50 mW/cm^2 at 33°C, 75 mW/cm^2 at 23°C and 33°C, and 100 mW/cm^2 at 23°C) in this histogram displayed a significant difference (p<0.05) in CES suggesting different levels of panniculus carnosus muscle injury. The highest average percent CES observed was

approximately 46% for rats that had undergone 94 GHz exposure delivered at 75 mW/cm^2 at 33°C ambient until death. The average time to death for this treatment was 43.8 minutes.

Figure 21: Comparison of the panniculus carnosus muscle response to prolonged 94 GHz MMW exposure applied under four conditions (50 mW/cm^2 33°C, 75 mW/cm^2 23°C, 75 mW/cm^2 33°C, and 100 mW/cm^2 23°C). The clear endomysial space (CES) of exposed and unexposed rat flank subdermal muscle was quantified by thresholding digital images of skin and values are presented as mean ± SD. The four exposure conditions resulted in significant differences in the panniculus carnosus CES (p <0.05) when compared to the unexposed side. Not shown is the comparison between 50 mW/cm^2 23°C exposed and unexposed tissue, which had no significant difference (n=3 for both exposed and unexposed side, p=0.263).

Overview photos of tissue for each treatment are seen in figure 22. Figure 22A and 22B represent tissue exposed to 94 GHz delivered at 50 mW/cm^2 for approximately one hour at 23°C and 33°C, respectively. In figure 22A, illustrated is regular collagen spacing and unperturbed muscle without retraction from the endomysium that is characteristic of injury from MMW exposure. In comparison, illustrated in figure 22B are high levels of vasodilatation (rectangle) and CES in the panniculus carnosus muscle (circle). Figure 22C and D represent tissue exposed to 94 GHz delivered at 75 mW/cm^2 for approximately one hour or until death at 23°C and 33°C, respectively. The 75 mW/cm^2 treatment at 23°C showed a widely variable response between experimental animals. Figure 22C is representative of tissue that underwent extensive injury during exposure. While injury was apparent in some of the collected tissue that underwent this treatment, other tissue was relatively unaffected. Panniculus carnosus muscle injury was highlighted by the high levels of retraction from the endomysium seen in figure 22C and D. Decreased collagen spacing (arrow) and extravasation (rectangle) evince high levels of injury in figure 22D. Thresholding comparisons were made between different power density treatments for the two ambient temperatures to quantify injury.
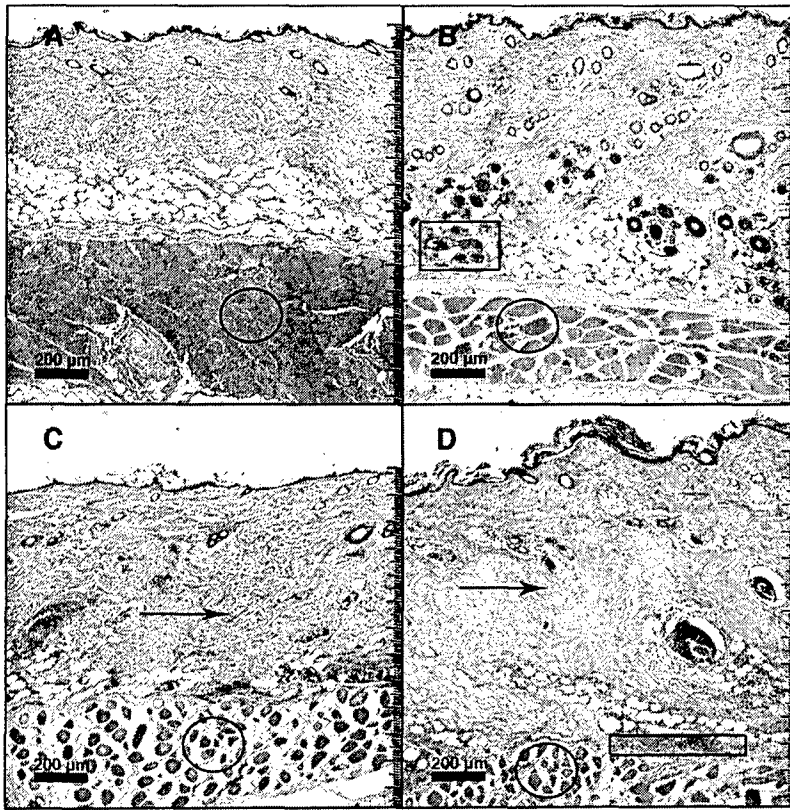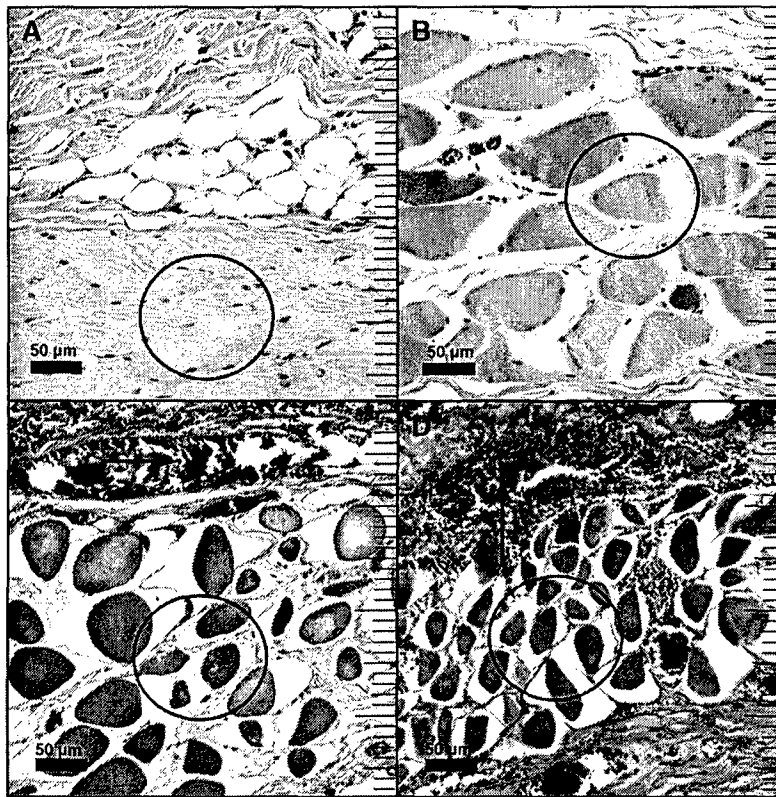
Figure 22: Histological overview of tissue response to prolonged 94 GHz MMW exposure applied under four conditions. Panel A and B) Tissue exposed to 50 mW/cm² at 23°C and 33°C, respectively. Encircled in A is muscle tissue that reveals no retraction from the supporting endomysium. However in Panel B, the circled area provides an example of muscle fiber retraction from the supporting endomysium resulting in a clear space (referred to as the CES). The muscle CES is characteristic of this exposure and indicates muscle injury. There is also notable vasodilation and some blood extravasation in B (rectangle). Panel C and D) Tissue exposed to 75 mW/cm² at 23°C and 33°C, respectively. Encircled is heavily injured muscle tissue demonstrating retraction from the endomysium. Notable is the decreased interstitium in the reticular dermis in D as compared to C (at arrows). Extravasation is indicative of extensive injury as seen in panel D (rectangle).

MMW Exposure Effects on Panniculus Carnosus Muscle

In further examination of the muscle layer located approximately 700 to 1000 μm directly beneath the skin, one can see a clear effect of prolonged MMW exposure. Displayed in figure 23 is the panniculus carnosus muscle layer at 10X the magnification seen in figure 22. The CES increased with both power density and ambient temperature. Where the 50 mW/cm^2 exposure at 23°C had little or no visible effect on the muscle (figure 23A), exposure to this same power density at 33°C increased CES as seen in figure 23B. Panels C and D of this same figure show tissue exposed to 75 mW/cm^2 at 23°C and 33°C, respectively. At 23°C, this power density sometimes caused notable myofiber retraction from the endomysium. In figure 23D, the muscle layer appears similar to figure 23C. Also noted in these two panels are obvious vasodilatation and extravasation observed in both exposure conditions.

Figure 23: Histology of panniculus carnosus muscle response to prolonged 94 GHz MMW exposure applied under four different conditions. Panel A and B) Rat panniculus carnosus muscle tissue exposed to 50 mW/cm^2 at 23°C and 33°C, respectively. Circled in A is muscle tissue exposed at 23°C ambient demonstrating no CES whereas tissue exposed at 33°C (circled in B) shows some retraction of fibers from the endomysium. Panels C and D) Muscle tissue exposed to 75 mW/cm^2 at 23°C and 33°C, respectively. Image C provides a more extreme example of the range of responses to exposure at 23°C and image D is representative of response to the exposure at 33°C ambient. Both panels show obvious muscle injury (circles) and vasodilatation (arrows).

Adipose tissue and epidermis

Displayed in figure 24 is adipose tissue and surrounding dermis for the power densities and ambient temperatures studied. Illustrated in figure 24B are examples of ruffled adipocytes.

Examples of vasodilation of the surrounding vasculature and high levels of extravasation are shown in figure 24B, 24C, and 24D. Depicted in figure 25 are characteristic epidermal layers for tissue exposed to the different power densities at either 23°C or 33°C. The blistering seen in figure 25D was observed in 2 of 4 experimental animals for the 75 mW/cm^2 33°C exposure condition. Because of variability in number, size, and injury to adipocytes and epidermis, the data collected concerning them were inconclusive. Some sources of this variability might include weight restriction of rats, epidermal injury from shaving, angle of cut during tissue preparation and other factors. Generally, there is more lysis of adipocytes and more blistering along the epidermis with increased power density and ambient temperature.
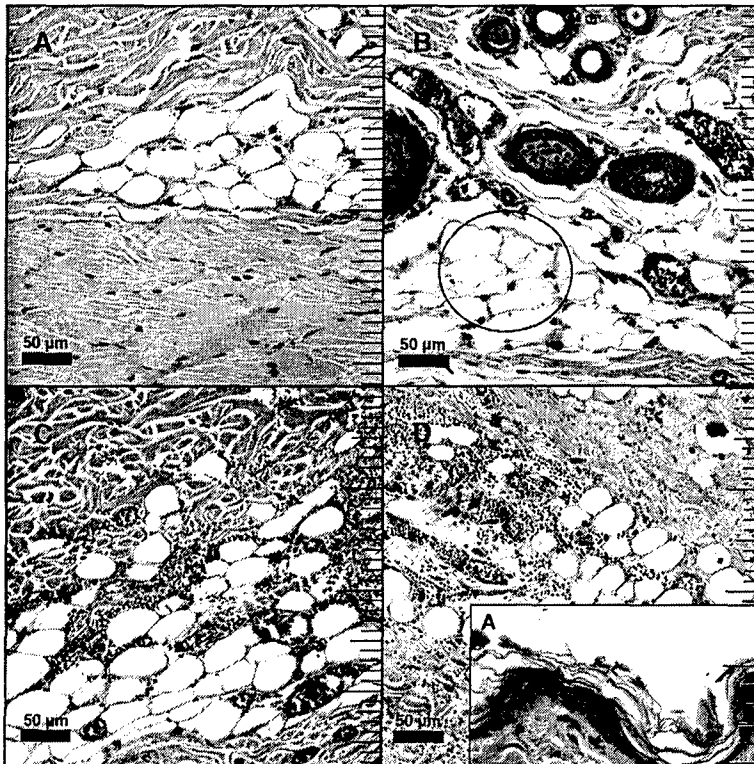
Figure 24: Histology of adipose tissue at the reticular dermis boundary following prolonged 94 GHz MMW exposure applied under four different conditions. Panels A and B) Adipose tissue of 50 mW/cm^2 exposed rats at 23° and 33°C, respectively. No appreciable effect is seen at 23°C while tissue exposed at 33°C ambient show ruffled adipocytes (circle) and support the notion of possible heat injury.

Panels C and D) Adipose tissue of 75 mW/cm^2 exposed rats at 23° and 33°C, respectively. There are no observed adipocyte responses to exposures made at 23°C or 33°C ambient; however, extravasation is clearly pictured in both panels.
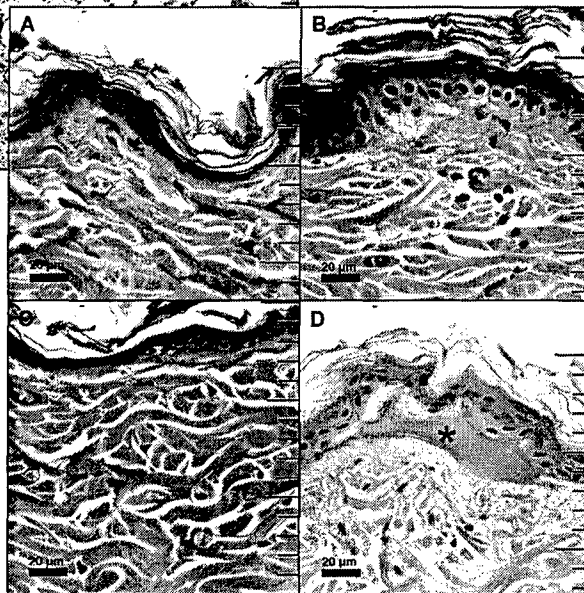
Figure 25: Histology of epidermal tissue response following prolonged exposure to 94 GHz MMWs applied under four different conditions. Panels A and B) Rat epidermis exposed to 50 mW/cm^2 at 23°C and 33°C, respectively. Panels C and D) Rat epidermis exposed to 75 mW/cm^2 at 23°C and 33°C, respectively. Blistering as shown in D at asterisk was observed in 50% of treated animals for the 75 mW/cm^2 at 33°C exposure (n=4).

Application of MMW energy

An alternative to examining temperature over time was to examine it as a function of energy applied to exposed animals. Furthermore, by calculating the difference between average surface, subcutaneous, and colonic temperatures for animals at different ambient temperatures after a known number of Joules/cm^2 have been applied, it was possible to quantify the amount of heat that animals at the higher ambient temperature were not able to disperse. Differences between average surface, subcutaneous, and colonic temperatures for 23°C and 33°C ambient, 50 mW/cm^2, 94 GHz exposed animals were calculated; calculations were repeated for 75 mW/cm^2, 94 GHz exposed animals at 23°C and 33°C ambient. These data are displayed in figure 26. Notably, the colonic temperatures for both comparisons began with a difference of about zero and increase linearly until the higher ambient temperature treated animals expired. The average colonic temperature difference between 50 mW/cm^2 23°C and 33°C treated animals at the time of death was 4.4°C. For 75 mW/cm^2 23°C and 33°C treated animals the average colonic temperature difference was 4.2°C at time of death. Because it is a lower power density, 50 mW/cm^2 exposed animals absorbed energy over a longer period of time than did 75 mW/cm^2 exposed animals. The 75 mW/cm^2 treated animals at 33°C ambient had an average time to death of 43.8 minutes (188 J/cm^2 applied) whereas the 50 mW/cm^2 treated animals at 33°C ambient average was 62.7 minutes (196.7 J/cm^2 applied).
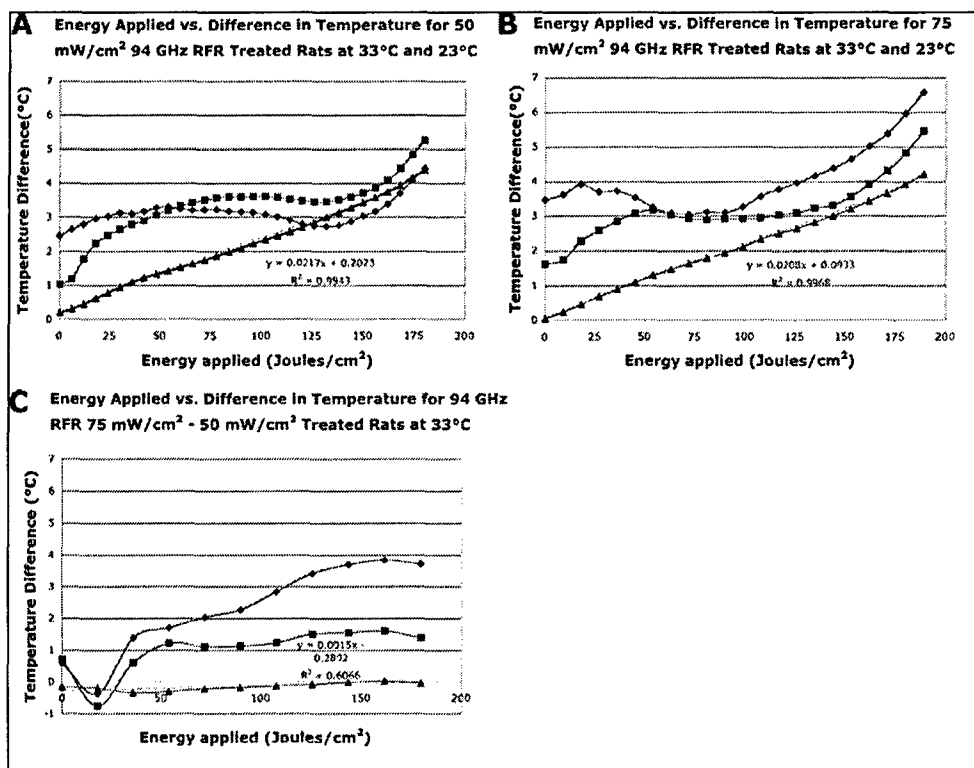
Figure 26: Temperature differences between rats during prolonged exposure to 94 GHz MMWs at 23°C and 33°C ambient. Surface (♦), subcutaneous (■), and colonic (▲) temperature differences were observed as more energy from MMW exposure was applied at 23°C or 33°C. A) 50 mW/cm^2 exposures at 33°C minus 23°C show an approximately linear difference in colonic temperature as energy is applied and a noticeable decrease in difference between surface and subcutaneous temperatures after approximately 120 J/cm^2 were applied. n=3 for both ambient temperature conditions. B) 75 mW/cm^2 exposures at 33°C minus 23°C show a similar linear increase in difference between colonic temperatures. Also notable is the decrease in difference between surface and subcutaneous temperatures after approximately 60 J/cm^2 applied. n=3 for both ambient temperature conditions. C) Temperature difference between 75 mW/cm^2 minus 50 mW/cm^2 treatments at 33°C shows that the difference in colonic temperature after a defined amount of energy is applied is approximately zero degrees. Differences between surface and subcutaneous temperatures increase with applied energy.

Quantification of changes in interstitium

Histograms in figure 27 display exposed (left) flank collagen and panniculus carnosus muscle injury, quantified as percent clear endomysial space in the muscle and percent interstitum in the dermis measured through thresholding analysis. Statistically significant comparisons are marked with symbols. As seen in figure 27B, quantification of clear endomysial space indicated that there was minimal injury to 50 mW/cm^2 23°C treated animals; all other treatments showed a significantly higher percentage of CES. The 10°C difference in ambient temperature had a profound effect on tissue disruption caused by the 50 mW/cm^2 exposure. Not shown are data indicating that there were no significant differences observed between 50 mW/cm^2 23°C exposed and unexposed side dermis interstitial space nor between 75mW/cm^2 23°C exposed and unexposed side dermis interstitial space despite qualitative observations indicating otherwise. That is, though the prolonged MMW exposed dermis appeared different than unexposed dermis under the microscope, the significance of this difference could not be confirmed
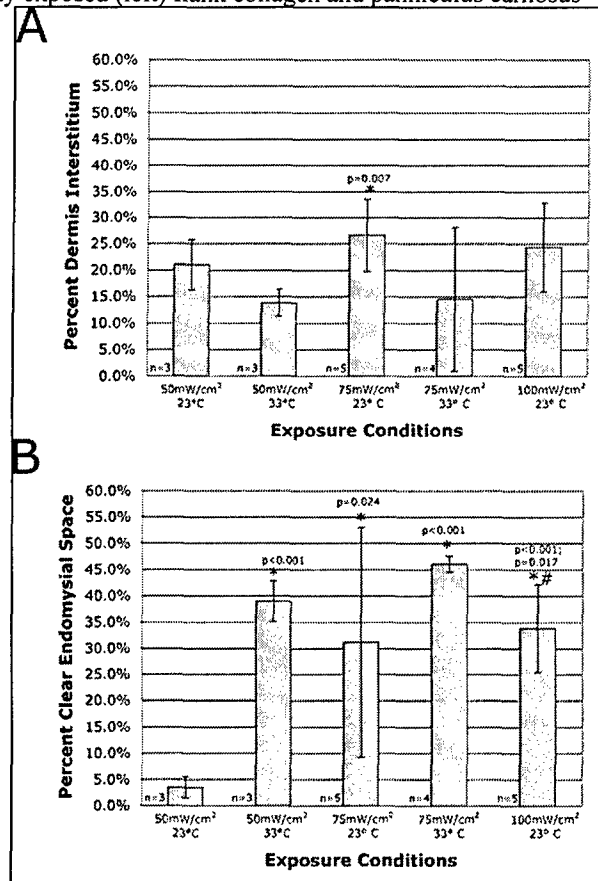
through thresholding and statistical analysis.

Figure 27: Comparisons of percent dermal interstitium and CES. Values presented are means ± SD. A) Thresholding quantification of dermis interstitium of treatments listed. Asterisk indicates a significant difference from the 50 mW/cm^2 33°C condition (p<0.05). B) Thresholding quantification of panniculus muscle clear endomysial space. Asterisk indicates a significant difference from 50 mW/cm^2 23°C condition (p<0.05) and pound indicates a significant difference from 75 mW/cm^2 33°C condition (p=0.017).

D and E) The effect of anesthesia on exposure response; passive heating effects

Some progress has been made on this objective. Preliminary results may be seen on figure 28.
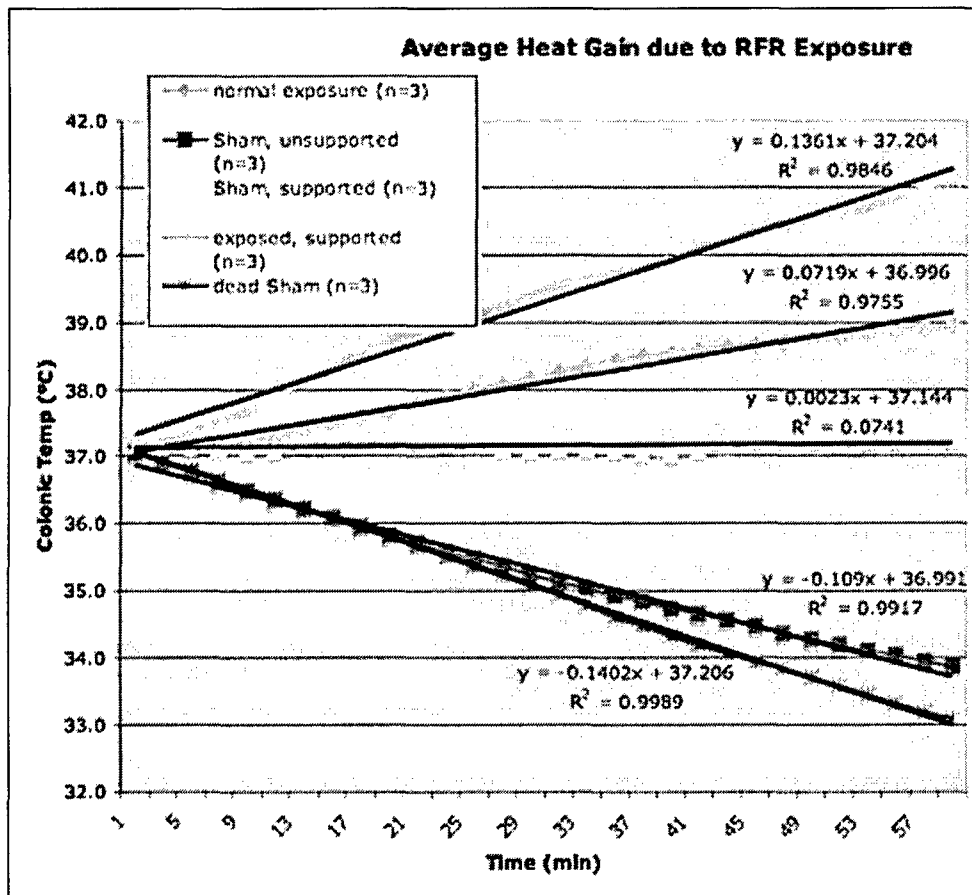
Figure 28: Effect of anesthesia and anesthesia heat support. The central yellow line represents an anesthetized animal with heat support. The red line represents a living anesthetized animal with no heat support. The green line represents an anesthetized animal with heat support and exposure to 94 GHz at 50mW/cm^2 at 23°C ambient. The blue line represents an anesthetized animals with no heat compensation and exposed to 94 GHz at 50mW/cm$_2$ at 23°C. And finally the purple (bottom) line represents the temperature loss of a dead animal. Regression lines are fitted to each plotted line.

These data indicate that a sham animal (anesthetized) dropped more than 3°C in body core heat during a typical 60 minute exposure period. A MMW exposed, anesthetized animal demonstrated slightly less than 2°C core rise. A heat-supported, MMW exposed, anesthetized animal demonstrated an almost 4°C rise in core temperature, which suggests that anesthesia depressed the body core response by approximately 2°C during the 60 minute exposure. A dead animal lost heat about 30% faster than an anesthetized animal. Passive heating data were collected but not sufficiently analyzed during the grant period to report here.

F) Thermograph correlation to histology

The antenna system that delivers the MMW to the target has a power dropoff of 50% at 7 cm from the center of the energy application. The distribution of the energy is Gaussian in nature over the target surface. Therefore if one where to examine tissue along the energy distribution, it might be possible to determine different tissue responses to different energy levels associated with the Gaussian distribution. Additionally as pointed out in the introduction to this section, the surface heating seen in the animal does not match the ideal target heat distribution. In other words elements of the anatomy of the animal perturb how the energy interacts with the surface. Figure 29 provides six examples of thermographs demonstrating a range of individual animal responses to the delivered MMW at two frequencies and power densities: 35 GHz at 100mW/cm^2 and 94 GHz at 75mW/cm^2.

94 GHz to 41°C colonic
PD = 75 mW/cm^2

35 GHz to 41°C colonic
PD = 100 mW/cm^2
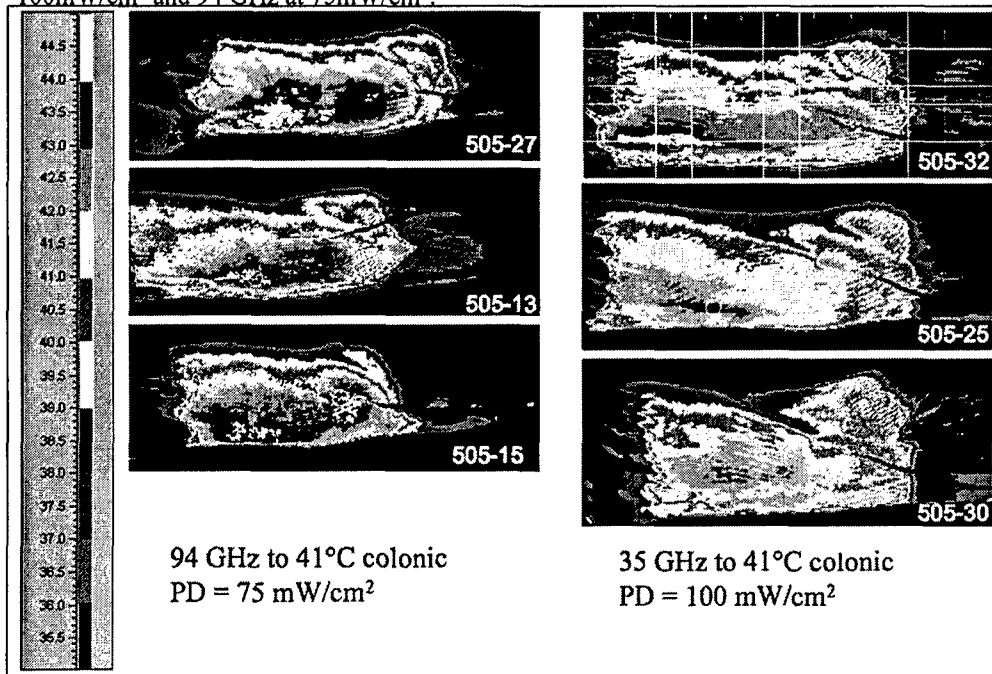
Figure 29: Thermographs at two frequencies and power densities. At left is a color heat gradient with temperatures above 44°C in white and temperatures below 36°C in black. The 94 GHz images at left appear smaller due to a different IR camera lens and optical working distance from animal. The 94 GHz animals have higher average temperatures than the 35 GHz animals as evidenced by more warm colors. Entering each image from the right is a black whisker, which represents the underling subcutaneous probe.

The upper left image (505-32) has a 1 by 2 cm grid drawn over the image. This grid corresponds to sampling of skin of similar size. The exposed skin was cut into 1 by 2 cm pieces corresponding to the thermograph. Each piece of skin was then examined and digital images

recorded and coded to the thermograph. This matrix then can be compared to the thermograph color corresponding to different delivered power density. This work is still on going at this time. Figure 30 is an example of the images and the corresponding thermograph. The purpose of the figure is to show the process; however, no detail can be obtained of these data.
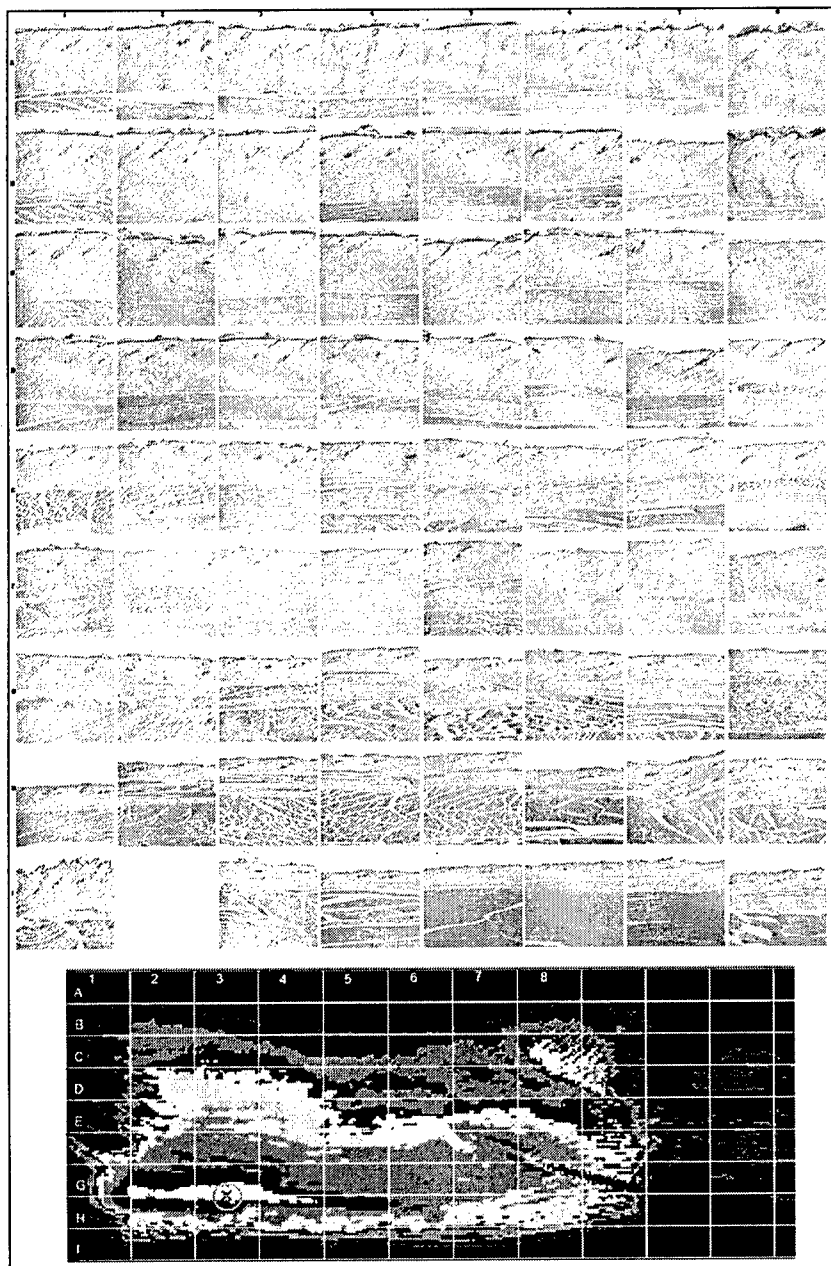
Figure 30: A 9 by 8, 1 by 2 cm histological reconstruction of a grided thermograph. The dorsal sections (top) have thicker skin than the ventral sections (bottom). Other differences are still being investigated.

G) Modeling MMW induced heart flow through skin.

The PI has a close working relationship with the FDTD modeling group at Brooks City-base. Colorized images such as the one found below (figure 31) are being provided to the FDTD modeling group for preliminary computation. These computations will be used as an initial part of a follow-on grant dealing with thermal modeling.
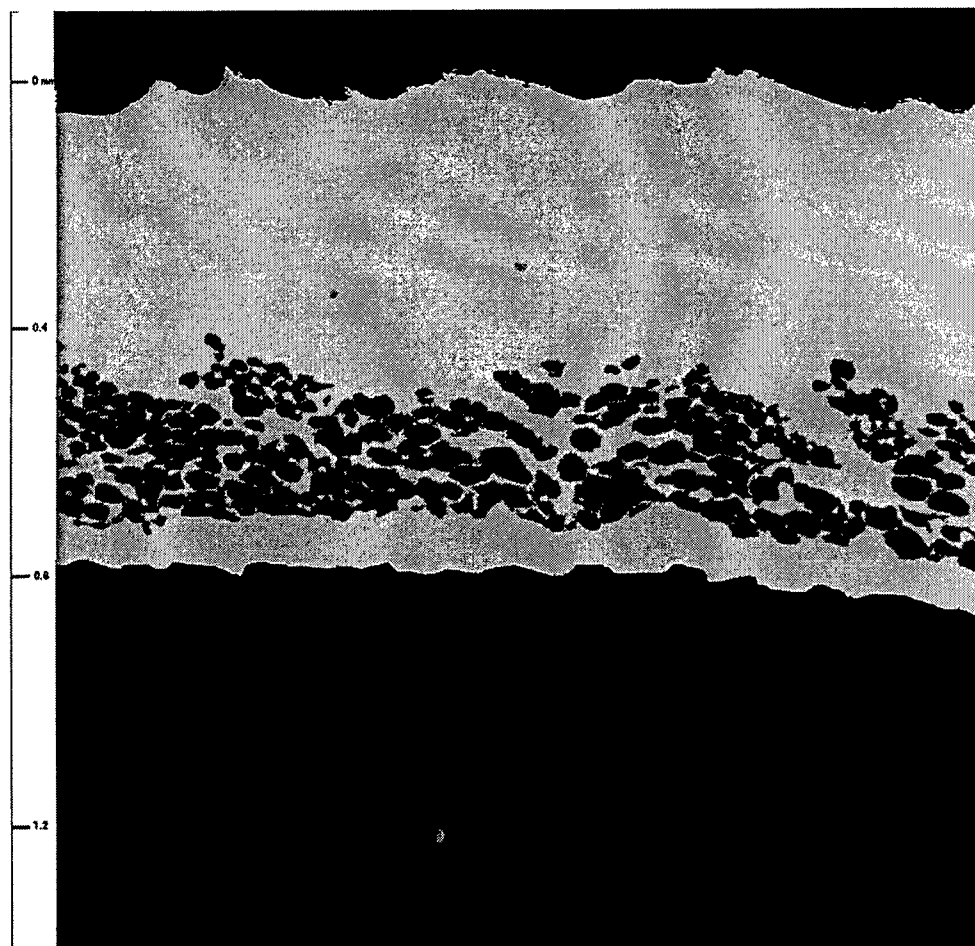
Figure 31: Colorized rat skin. A representative section of rat skin was selected for pseudocoloring. A millimeter scale is at left. The rust brown at top is the air interface with the skin surface. The lighter blue beneath is the epidermis. The yellow orange is dermis. The several small lighter blue dots are blood vessels. The red areas represent adipocytes. The dark blue at bottom is the hypodermis including muscle. The pixel values of the image were selected to correspond to algorithms being used to calculate SAR through the FDTD program. The

thermograph work described in the preceding section will guide efforts to select the most representative images for thermal modeling.

James Weaver Subcontract

At the onset of the research period the PI had a working relationship with Dr. James Weaver. Dr. Weaver has a broad research program dealing with pulsed MMW energy and well as continuous MMW energy. He has interests in both cellular responses to RFR as well as whole animal reaction. Recently he and his collaborators have published their results incorporating all of these interests in Stewart et al. 2006. Excerpts of report that pertain to this study are found below.
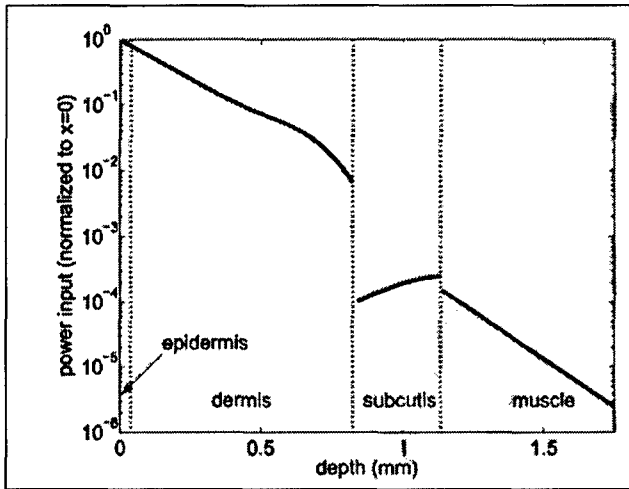
Four layers of skin and hypodermis are depicted in this graph. Electrical conductivity and permittivities were obtained from the literature. The discontinuities are associated with dielectric property change. "Multiple internal reflections within the dermal and fat layers result in the deviation of the profile from a simple exponential decay shape."
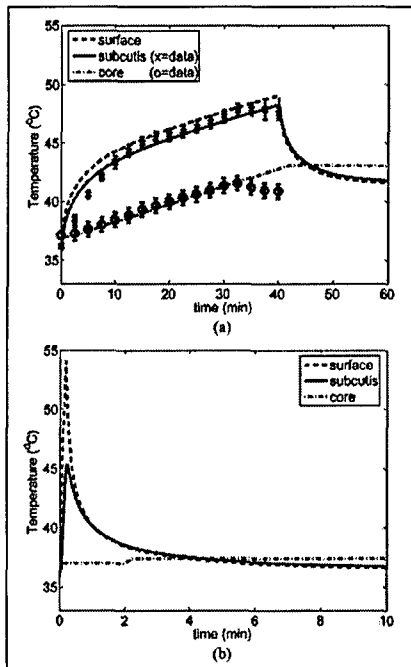
Figure 32: Power absorbed in the skin tissue from applied 94 GHz exposure.

Compare the A panel at upper left to figure 6B. At left is the thermal model for 94 GHz at 75 mW/cm^2 to 40 minutes. The core temperature is similar although higher than actual. The model also predicts a peak at 30 minutes, which is not seen in actual data. Both the surface and subcutaneous temperatures are nearly six degrees higher in the model than actual. It might be the case that the temperature drop associated with anesthesia use covers the full extent of temperature rise in the measured actual data.

The lower graph at left models the response to 1 W/cm² exposure for 10 seconds.

Figure 33: "Model for subcutaneous and colonic temperature for an anesthetized rat exposed to 94 GHz."
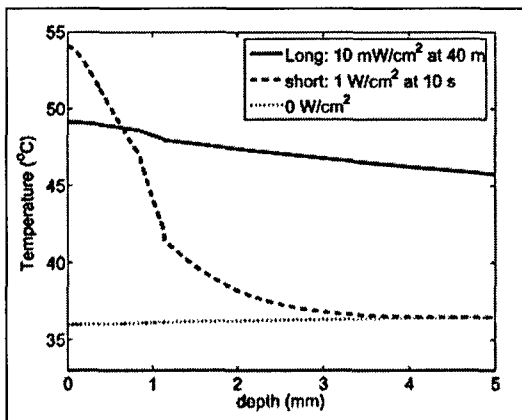
The graph at left compares a 40 minute application of a 75mW/cm² power density to that of 1W/cm² per 10 seconds. The short exposure is hotter faster and cooler quicker that the longer exposure at lower power density.

Figure 34: Temperature depth profile resulting from exposure to 94 GHz at two power densities and exposure time applications: 40 minutes at 40mW/cm² and 10 seconds at 1 W/cm².
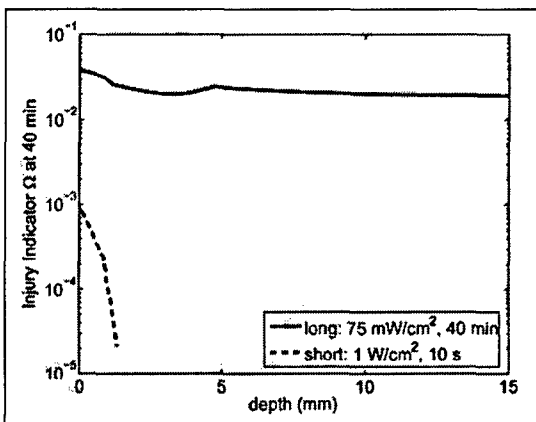
Weaver's group has developed an injury index based upon several factors: the Arrhenius constant, birefringence loss of rat skin collagen, an injury threshold, complete epidermal necrosis equals 1, and values associated with the burn literature. The main premise behind the injury index is a transition from the native to denatured molecular state. They cite electrical shock literature that indicates the injury threshold is 42°C. We have calculated different multiple injury thresholds based on histology as seen in figure 13. The data at

left indicates low power long duration exposure produces more damage than high power short duration exposure

Figure 35: Cumulative thermal-injury indicator for two exposure conditions. (above)
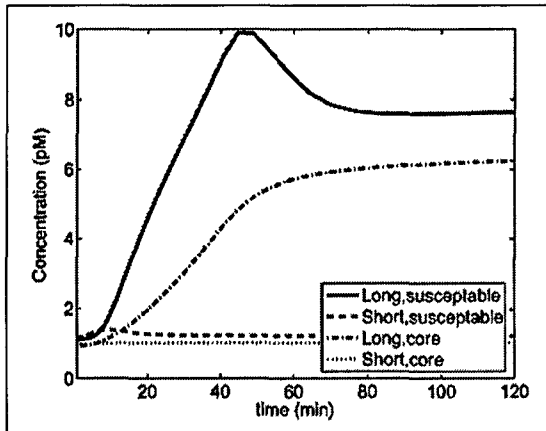
Weaver's group theorizes that a substance called "s" is released by MMW exposure. This material is presumably from the epidermis and is transported through the skin. The lower power density long exposure duration releases more of this material than does the high power density short exposure. The "s" moves through the body and is removed with time. The material might fit Jauchem's [2006] recent report about autocoid release.

Figure 36: Substance "s" in susceptible muscle layer and blood stream and clearance times.

David Nelson Subcontract

During the last year of the research period the PI had a working relationship with Dr. David Nelson. Dr. Nelson's efforts are contained in a report found below.

Development of a Model of Millimeter Wave Energy Absorption in the Skin of the Rat

D.A. Nelson
Department of Biomedical Engineering
Michigan Technological University
Houghton, MI 49931

The objective of this effort is the development of a numerical model which will enable the prediction of surface and sub-surface tissue temperatures in the skin of the rat, during continuous-wave (CW) exposure to radio frequency (RF) radiation of millimeter wave (MMW) frequency (30 GHz – 300 GHz). Due to the small length scales involved, this demands a high-resolution model which reflects tissue heterogeneity and its effects both on RF energy absorption and heat transfer. The thermal model (under development) must also reflect heat transfer effects of blood flow and metabolism.

The preliminary effort, described in this report, was to develop a one-dimensional model which will enable calculation of local energy absorption rates (SAR) in skin which is exposed to MMW radiation. Two versions of a one-dimensional finite-difference, time domain (FDTD) code have been developed. The FDTD method is a well-established technique for estimating energy absorption in tissue exposed to RF radiation [1]. All computer codes were written in Matlab 7.1 (Mathworks Inc., Cambridge, MA).

The first model describes the skin as homogeneous, dermal tissue. The second version is a three-layer model of tissue: epidermis, dermis, and fat. A separate computer code was written for the purpose of estimating the permittivity constant and the [electrical] conductivity of each tissue, based on their water content. This program implements a Cole-Cole dispersion model [2,3] to determine those properties as functions of RF frequency. The Cole-Cole parameters were obtained from the literature [4-6]. Results for the entire MMW band are shown as Figure 1. For this preliminary model, the epidermis was considered "dry", and the dermis "wet" tissue.

Table 1 shows the calculated permittivity (farads/m) and conductivity (siemens/m) values of the tissue layers at 35 GHz and 94 GHz.

Table 1. Permittivity and Conductivity of tissue layers, as calculated from the Cole-Cole model.

	35GHz		94GHz	
	Permittivity (F/m)	Conductivity (S/m)	Permitttivity (F/m)	Conductivity (S/m)
Dry Skin: Epidermis layer	13.1	28.1	5.66	37.2
Wet Skin: Dermis layer	15.7	30.4	7.51	45.4

Fat (Infiltrated):
Subcutaneous Fat   5.57   6.00   3.74   10.4
      layer

FDTD Models

Homogeneous tissue model. A model of continuous wave (CW) irradiation of homogeneous tissue (dermis) was developed. The purpose of this model was to compare results with those published in the literature, and to provide a basis for comparison of results from heterogeneous models. It also enables determination of an appropriate scale for future models; i.e., it is necessary to know how deep energy penetrates in order to establish the domain of the model.

Results from the one-dimensional, homogeneous FDTD simulation are shown as Figure 2 for (a) 35 GHz exposure and (b) 94 GHz exposure. Normalized SAR values are expressed in units of $(W/kg)/(W/m^2)$. For example, for an incident RF power density of 1 W/m^2 at 35 GHz, the SAR at the skin surface is approximately 1×10^{-3} W/kg. At a tissue depth of 0.05 cm, the SAR has decreased by an order of magnitude. The decrease in SAR with tissue depth is even more drastic at 94 GHz. This is consistent with the physical principle that higher frequencies generally produce shallower penetration.

The tissue penetration depth is defined as the distance at which the power density has been attenuated to 13.5% (or e^{-2}) of its incident value. Based on this homogeneous FDTD model, the RF tissue penetration depth is 4.0×10^{-2} cm at 35 GHz and 3.6×10^{-2} cm at 94 GHz.

Heterogeneous tissue model. A one-dimensional, heterogeneous (three-layer) tissue model was developed for a 4-mm thick . The thickness of each layer is shown in Table 2. The model used a grid spacing of 20 μm.

Table 2. Thicknesses of layers for the heterogeneous skin model.

	Epidermis	Dermis	Subcutaneous Fat
Thickness, μm	40	920	3040

Results from the heterogeneous model are shown in Figure 3. Epidermal SAR values are comparable to, but slightly higher than those obtained from the homogeneous model. Note also the abrupt drop in SAR at the dermis/subcutaneous fat interface. This suggest the thickness of the dermis may be an important variable in determining the effective SAR in the skin.

Estimates of the penetration depth for the heterogeneous model are 7.8×10^{-2} cm at 35 GHz, and 4.0×10^{-2} cm at 94 GHz. Those values are consistent with estimates published in the literature [7].

The estimate for 35 GHz generated by the heterogeneous model is substantially greater than the value obtained from the homogeneous model, while the two estimates at 94 GHz are within 10% of each other. This implies the effects of tissue non-homogeneity may be more significant at shorter wavelengths within the MMW band.

Thermal Model. Development of a finite-difference heat transfer model is in progress. That model will incorporate FDTD calculations of local SAR for each node in the model. The initial model will treat blood flow as a distributed thermal source/sink. That will facilitate study of the effects of the depth of the vascular plexus on heating of the skin, independent of effects from individual vessels.

References

1. Sullivan, D M and Borup, D T (1987) Use of Finite-Difference-Time-Domain Method in Calculating EM Absorption in Human Tissues. *IEEE Trans. Bio-med. Eng. Vol-BME-34, No-2, Feb-1987.*

2. Cole, K and Cole, R H, (1941) Dispersion and Absorption in dielectrics. Alternating current characteristics. *J. Chem. Phys.9 341-51.*

3. Tamura, T, Tenhunen, M, Lahtien, T, Repo, T and Schwan, H P (1994) Modelling of dielectric properties of normal and irradiated skin. *Phys. Med. Biol. 39 927-36.*

4. Gabriel, C, Gabriel, S and Corthout, F (1996) The dielectric properties of biological tissues:I . Literature survey. *Phys. Med. Biol. 41 2231-49*

5. Gabriel, S, Lau, R W and Gabriel, C (1996) The dielectric properties of biological tissues: II. Measurement in the frequency range 10 Hz to 20 GHz. *Phys. Med. Biol. 41 2251-69*

6. Gabriel, S, Lau, R W and Gabriel, C (1996) The dielectric properties of biological tissues:III. Parametric models for the dielectric spectrum of tissues. *Phys. Med. Biol. 41 2271-93.*

7. Gandhi, O and Riazi, A (1986) Absorption Of Millimeter Waves by Human Beings and Its Biological Implications, *IEEE transaction on Microwave Theory and Techniques, Vol. MTT-34, No. 2 , Feb. 1986.*

(a)
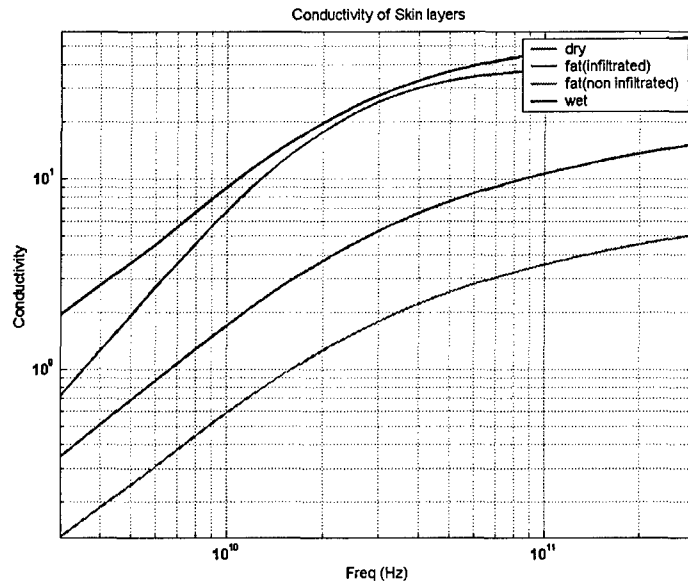
(b)
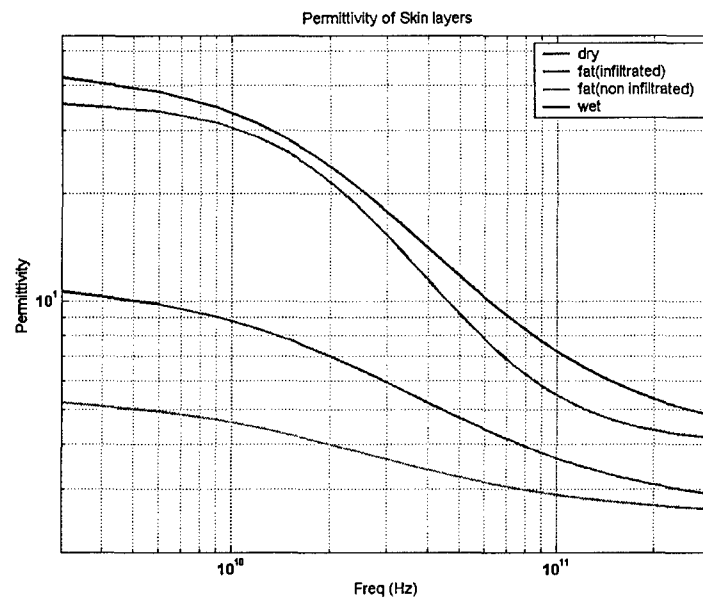
Figure 1. The estimated conductivity (a) and permittivity (b) of skin tissue is shown for the frequency range $30\,\text{GHz} < f < 300\,\text{GHz}$. Values were calculated from a Cole-Cole model, based on water content of the tissue.

(a)

(b)
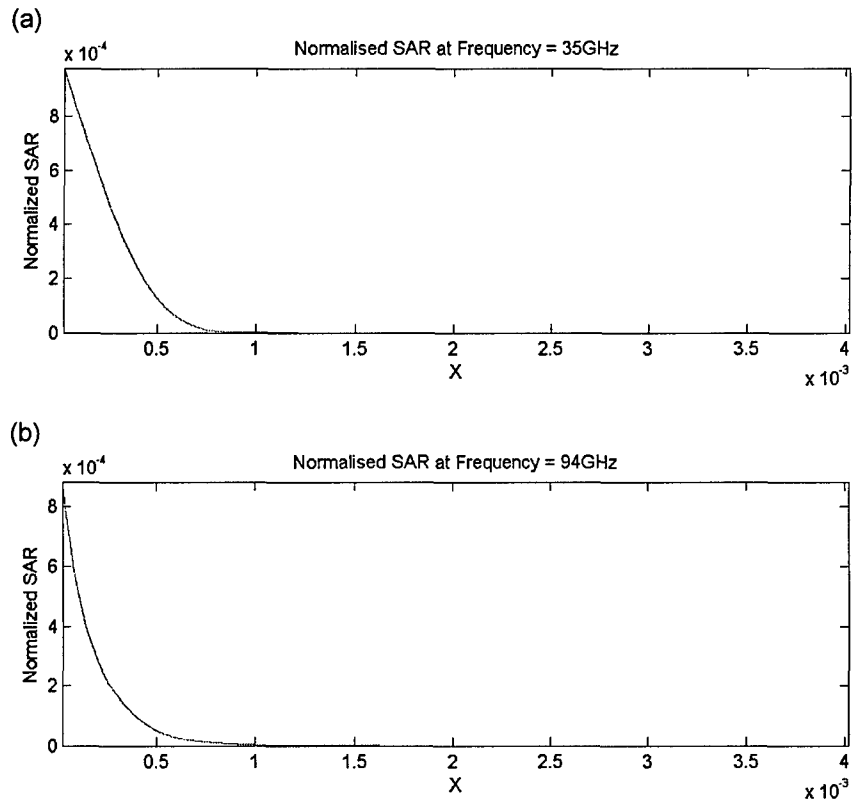
Figure 2. Normalized SAR is shown as a function of depth into the tissue for two incident RF frequencies: (a) 35 GHz; (b) 94 GHz. Normalized SAR is expressed in units of $(W/kg)/(W/cm^2) \times 10^4$. Note values have been multiplied by 10^{-4}. Tissue depth is expressed in $m \times 10^{-3}$ (i.e., millimeters).

Figure 3. Normalized SAR values were calculated as a function of depth
into the tissue for a 3-layer model of the rat skin.

Discussion:
A) Relationship of Power Density to tissue response to 94 GHz

The objective of our investigation was to understand the effects of increasing power density on skin tissue response to 94 GHz MMW. The effects of MMW exposure are largely in re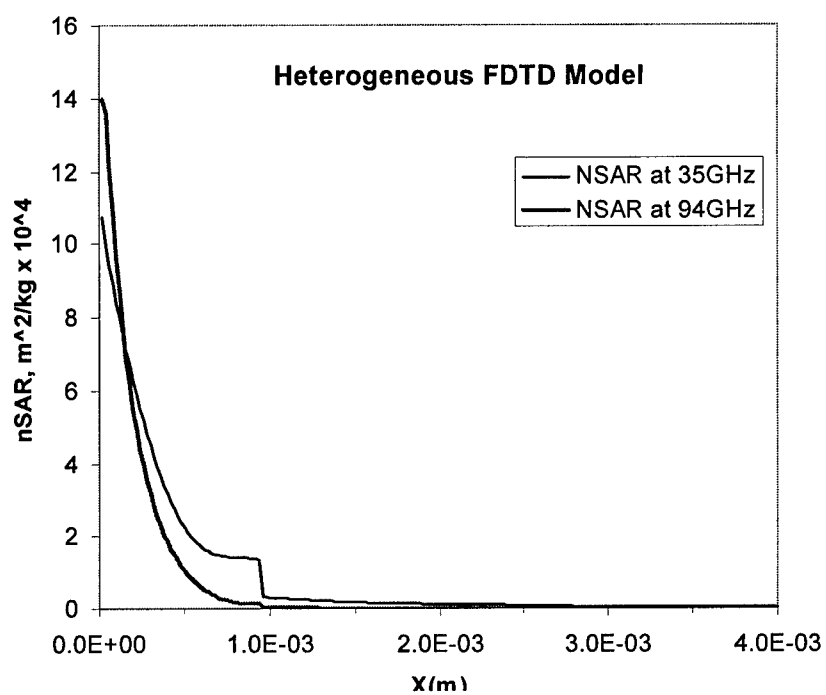sponse to its thermal effects. As the duration of exposure time increases, the energy and thus the heat also increase in a controlled manner until the protective measures of thermoregulation fail to compensate leading to an uncontrolled rise in body temperature [Johnson and Guy 1972]. Budd [1985] suggested that MMW burns may involve deep tissue and have longer latent times for observation. Section B of this report describes the effect of recovery duration time after exposure to 94 GHz MMW on observed tissue injury. In addition, the properties of the tissue such as dielectric constant affect the absorption of MMW energy. Johnson and Guy [1972] further suggested that the energy absorption is highest in tissues with high water content such as muscle and skin, but low in areas of low water content such as fat and bone.

We found that the temperature response to the MMW exposures in our experiment occurs in essentially two stages (figures 5 and 6). In the first stage, rapid temperature increase occurs over the first ten minutes of exposure for both the surface in subcutaneous tissue regions (figure 5 A,B). At this point the body of the animal has not responded to the excess heat load effectively. If the animal is unable to respond efficiently to the excess heat from the MMW exposure injury to the tissue can occur. The second stage of temperature response to MMW exposure occurs after the first ten minutes when the rate of temperature rise decreases in both the surface and subcutaneous regions shown in figure 5 A,B. This suggests that the body of the animal is attempting to adjust to the excess heat. The ability of the animal to control the temperature rise via cooling methods of the tissue was suggested by Johnson and Guy [1972]. Erwin [1983] suggested some of the mechanisms activated by excess body heat including cutaneous vasodilation, increased respiration, and decreased metabolic activity.

The graphs demonstrate in figure 1 that higher power densities correspond to higher temperatures than lower power densities. Figure 6 shows the same temperature data arrayed by power density. Graph 6A shows that in response to the 50 mW/cm^2 exposure the surface and colonic temperatures are essentially equal. The equal temperature values for the surface and colonic regions suggest that the animal is able to handle the excess heat load efficiently by spreading the heat essentially equally over all the regions. Although the subcutaneous temperature is slightly higher than the surface and colonic temperatures, the difference in temperature is very small.

Alterations in skin blood flow are the primary mechanisms for removing excess heat from the skin and transferring it to the core [Walters et al. 2004]. This is supported by the decrease in rate of temperature change in both the surface and subcutaneous regions and at the same time an increase in rate of temperature change in the colonic region after the first ten minutes of exposure (see figures 5 and 6). The convective ability of the vascular system to respond to the heat and channel it to the rest of the body is the primary mechanism the body incorporates to control skin heating. Foster et al. [1978] described heat transport by the blood becoming more pronounced over time in response to 94 GHz MMW; supporting our finding that the rate of temperature change in the surface and subcutaneous regions decreases after the first ten minutes of exposure.

The ability of the vascular system to respond to excess heat load is also supported in our study by the dilation of the blood vessels observed at the higher power density exposures (75 and 100 mW/cm^2) seen in the histological images shown in figures 7 and 9 and suggested by the

graphs shown in figures 12 and 13. A secondary mechanism of heat transfer to the core is via conductance through the muscle and fat layers [Adair and Black 2003]. The ability of the body to regulate its temperature range is ascribed the term thermoregulation [Adair and Black 2003]. The increased slope of the colonic temperature in figures 5 and 6C suggests the transfer of heat energy from the surface and subcutaneous regions to the colonic region via the circulatory system.

Jauchem et al. [1999] found that circulatory collapse occurs at 94 GHz 75 mW/cm^2 after a period of 38.8 minutes for unshaved rats and 41.1 minutes in shaved rats. Specifically, Jauchem et al. [1999] found that 94 GHz cause extreme heating in the peripheral tissue; however, the colonic region responds to a much lower degree. Our results of cutaneous vasodilation and extravasation in response to MMW exposure support the possibility of eventual cardiovascular failure if continued exposure was to occur; however, in our study the animals exposed at all three power densities (94 GHz; 50, 75, and 100 mW/cm^2) survived for the full 60 minutes exposure time upon which they were sacrificed with CO_2 asphyxiation. This suggests discrepancies in data between the two studies, but it is necessary to note that Jauchem et al. [1999] used a ketamine injection anesthetic while our study used the gas anesthetic isoflurane. The effects of anesthetics on the physiological response to MMW are a topic of interest for the future.

The histological response the MMW exposures, observed in figures 7-10, are most likely in response to the thermal effects of the MMW exposures. If the animal is unable to compensate for the heat increase, when the thermoregulatory ability of the animal can no longer compensate for the excess heat, deleterious changes may occur in the tissue [Erwin 1983; Johnson and Guy 1972]. An injury score was assigned to each exposure and are seen in figure 12. The graph shows much higher injury scores in the 100 mW/cm^2 exposures as compared to the 50 mW/cm^2. In addition four of the 75 mW/cm^2 show high injury scores (above 5) while two of the 75 mW/cm^2 exposures show small injury scores similar to the 100 mW/cm^2. This is consistent with the idea of 75 mW/cm^2 being in the threshold for injury response at 94 GHz exposures for 60 minutes. Possible explanations for the reason that only some of the 75 mW/cm^2 animals reached the temperature threshold for injury response can include differences in physiology, metabolism, and weight (see figure 13).

The most significant response to increasing MMW exposure power densities is increased clear endomysial space (CES) in the panniculus carnosus muscle as shown visually in figures 7 and 10 and graphically in figure 11C. The response by the muscle was not initially expected because the majority of the 94 GHz MMW penetrates to a depth of approximately 400 µm [Blick et al. 1997; Ryan et al. 2000]. The distance between the epidermis and panniculus carnosus muscle was measured using a micrometer and was found to be approximately 900 µm (see figure 11A); deeper than the reported value of MMW penetration.

The most significant histological response observed in response to exposure at high power densities is increases in the clear endomysial space. The digitial images shown in figures 7 and 10 show muscle that has retracted from its supporting endomysium (connective tissue). The excess space surrounding the space in response to the MMW exposures is likely due to an increased fluid build up between the fibers (edema) and more importantly the degradation of the connections between the muscle protein and connective tissue. In addition the striations that traditionally accompany skeletal muscle is not evident in the atrophied muscle suggesting muscle protein degradation.

Measurements of the percentage clear endomysial space (CES), as shown in figure 11C, quantify the muscle response to MMW exposure. The CES is significantly higher in both the 75 mW/cm^2 and 100 mW/cm^2. The standard deviation observed for the exposed 75 mW/cm^2 is quite large which suggested that a threshold of response existed at the 75 mW/cm^2 power density. Two of the animals at the 75 mW/cm^2 power level did not reach the threshold temperature of 42.1°C (see figure 13) that is needed for the denaturation of muscle fibers and their retraction from the associated endomysium which would leave the clear endomysial space. The other four animals at this power level did reach the threshold value of 42.1°C for muscle response and was evident histologically. All of the 100 mW/cm^2 exposures remained above the threshold of muscle damage, while the 50 mW/cm^2 exposures all remained below the threshold of muscle response.

As a group we were surprised by the response that the muscle layer underwent in response to the MMW exposures. The muscle layer was measured to have an average depth from the epidermis of approximately 0.9 mm. This depth is much lower than the reported value of 0.4 mm for MMW penetration by Blick et al. [1997] and Ryan et al. [2000]. This suggests that there must be a secondary mechanism caused by the MMW exposure to cause muscle response at this depth. We attribute the mechanism to the distribution of heat via convection through the circulatory system as explained previously.

A study by Clark et al. [1984] described the accelerated protein and glucose catabolism in skeletal muscle in response to distant thermal injury in humans. Odessey and Parr [1982] also found that protein degradation in muscle occurs in response to thermal burns; however, it is of note though that typical thermal burns occur from the epidermis (outside) towards the dermis (inward) whereas MMW burns are unique originating from the inside and proceeding in a Doppler fashion outward. In both cases the vascular system is able to disperse heat away from the source supporting the idea that the thermal effects of MMW exposure are responsible for the muscle atrophy.

In addition to muscle injury response several other responses were identified. Blood vessel dilation and extravasation were seen in many of the tissues in which muscle response was observed. This supports the idea that the vascular system is responsible for transferring the excess heat to the muscle. Data shown in figure 11 A,B suggest that the dermis is responding in some way to the exposure. Although not significant the graph shows that the exposed tissue side is consistently higher in percentage of interstitial space than the unexposed side. This suggests that edema and extravasation are increasing the fluid between the collagen bundles. It is also possible that changes in the collagen fibers are occurring, but this cannot be confirmed at this point. The depth of the dermis is highly variable and likely associated to the period of the hair cycle in which the animal is exposed [Chase et al. 1953].

Thresholds for extravasation, blood vessel dilation, and blistering were also identified and are shown in figure 13. Johnson and Guy [1972] reported that local effects of tissue heating include: increases in blood flow due to arteriolar and capillary dilation, and possibly greater capillary membrane permeability. It was found that the threshold for both blood elements were found to have a critical temperature value of the same value of 42.9°C. Only one of the animals exposed at 75 mW/cm^2 showed vascular response to the 94 GHz exposures, while all the 100 mW/cm^2 showed vascular response. The value of the thresholding data comes in the predictive form. It suggests that a temperature threshold is required for tissue injury response to occur, and is not directly dependent on the power level of exposure.

The thresholding data suggests that regardless of power density it can be expected for muscle injury to observed if the average maximum surface and subcutaneous temperature reaches 42.1°C. This is also the case for the blood elements (vessel dilation and extravasation) as well as blistering with thresholds of 42.9°C and 44.1°C respectively. Although in our experiment the 50 mW/cm^2 did not show any tissue response, the thresholding data suggests that if a length of exposure time was sufficient to reach the threshold temperature then the injury would be expected to be observed. It is important to note that what injury response is observed in response to MMW exposure depends on several factors including: power density, length of exposure, metabolic activity of the animal, weight of the animal, period of hair cycle in which the animal was exposed, and physiological activity of the animal.

B) Exposure time variation and recovery time variation to 94 GHz
Exposure Duration
Histology

Previous studies have shown that MMW-induced tissue heating may result in injury if temperature rise is high and long enough [Erwin 1983; Roberts et al. 1986]. The previous section demonstrated that 60-minute exposures to continuously applied 94 GHz at power densities of 75 and 100 mW/cm^2 caused significant injury in the skin, especially in the panniculus carnosus muscle, which is the most sensitive to applied MMW. The study also demonstrated that the injury escalated in animals exposed at a power density of 100 mW/cm^2. Thus, histological alteration was proportional to the increase in temperatures associated with the increased power density.

The first part of this study was aimed at tracing the path of injury development on the skin at fifteen-minute intervals of a full 60-minute exposure to 94 GHz and two power densities at 23°C ambient. Such knowledge would provide information on what power density, what duration, and the amount of energy necessary to create a specific level of injury. Rather than simply concentrating on physiological data to examine the effects of MMW, we studied the histology of the exposed animals to have a visual representation of the effects of MMW on the skin and underlying tissue.

Animals exposed at 75 mW/cm^2 demonstrated no significant injury of the skin until an accumulated 60 minutes of continuous exposure. Although some slight change in the dermal collagen was observed at 45 minutes, it was clear that it took an exposure of at least 60 minutes to result in significant injury of the dermis and the muscle, illustrated in figure 14D. The panniculus carnosus muscle layer seemed to be most sensitive to MMW, and although the exact reason is not known, it is known that MMW absorption is highest in tissues with high water content such as muscle [Budd 1985; Adair and Petersen 2002]. This suggests that tissues with properties sensitive to MMW that are well beyond the penetration depth of high frequency MMW are still highly susceptible to injury. Not all of the animals exposed for 60 minutes displayed the same level of injury. Less than half of the animals did not display injury of the skin. This observation suggests that thermoregulatory mechanisms in the animals that conduct heat in and out of the body play an important role in the level of injury sustained. It may also indicate that it takes time for some injury to become apparent. Thus, skin response post-exposure was explored and reported in the second part of this paper.

The histology of animals exposed at a power density of 100 mW/cm^2 clearly demonstrated a progression of injury with increasing time of exposure (figure 15). The experiment demonstrated that even a fifteen-minute exposure at 100 mW/cm^2, which at a power

density of 75 mW/cm^2 had no effect, began to affect the muscle layer. Animals exposed for 60 minutes did not survive the exposure and their histology displayed significant injury (figure 15D).

The histology of animals exposed at 75 mW/cm^2 and 100 mW/cm^2 allowed us to visualize the anatomical injury resultant from MMW, measure the time and energy needed to affect the skin, and discover whether the heat load and injury was handled in a gradient or threshold style of change in anatomy. In addition, it allowed us to conclude that as power density increases, injury development is quicker and more profound and that the effects of MMW are not limited to surface tissue as expected but evident in deeper tissue.

The effects of MMW on deeper tissues may be affected by the conduction of heat to surrounding tissue and heat movement through perfusion (blood flow) [Nelson et al. 2000; Xiao-feng and Anying 2003; Gowrishankar et al. 2004; Alekseev et al. 2005]. Studies on heat transfer in biological systems exposed to MMW have shown that the thermal energy delivered by MMW stimulates tissue to increase blood flow by thermoregulation in order to remove the excess heat [Xiao-feng and Anying 2003; Gowrishankar et al. 2004]. Walters et al. [2004] studied the relationship between skin blood flow and skin temperature rise in human subjects exposed to 94 GHz at a power density of 175 mW/cm^2 and at 23°C for 180 seconds. The data indicated that an increase in skin blood flow during MMW exposures decreased the rate of surface heating and resulted in a steady-state condition in which the energy input due to exposure was matched by a convective outflow due to a corresponding increase in skin blood flow. By occluding blood flow and then restoring it, it was found that the steady-state condition in skin temperature was indeed dependent on an increase in skin blood flow [Walters et al. 2004]. Thus, the greater ability of the human skin vasculature to vasodilate in response to MMW results in the effective removal of heat from the skin before thermal damage occurs in human subjects exposed to low power density (175 mW/cm^2) for 2-3 minutes.

The temperature data of the rats in this study suggest that blood flow may also play an important role in heat transfer and in the reduction of heat, although a role not as significant or efficient as in human subjects. Since this study consisted of longer exposure periods (15, 30, 45, and 60 minutes) than Walters et al. [2004], heat transfer through the vasculature of the rats was allowed time to become significant. Thus, longer exposures at a lower power density (75 and 100 mW/cm^2) MMW do not necessarily result in lethal injury in rats if thermoregulatory mechanisms such as increased blood flow come into play.

In terms of energy applied (power density multiplied by exposure time), exposures to 94 GHz 75 mW/cm^2 at 23°C ambient required at least 270 joules to affect the skin significantly. Injury from exposure at power density of 100 mW/cm^2 was evident with the application of 90 joules at 15 minutes and escalated with increasing energy corresponding to the remaining fifteen-minute intervals.

Temperature Analysis

Changes in surface, subcutaneous, and colonic temperature rates in exposures to 75 mW/cm^2 indicated a that MMW heat moved from compartment to compartment (skin to subcutaneous, to body core). Temperature changes in exposures to 100 mW/cm^2 also resulted in a similar although not identical heat movement. Figures 16 and 17 illustrate that heat flowed from the surface to subcutaneous tissue and finally to the body core, in accordance with previously observed results of 94 GHz exposures [Jauchem et al. 1999; Millenbaugh et al. 2006]. The figures also defined the time it took for heat to be transferred.

The data for animals exposed to 75 mW/cm^2 demonstrated that two minutes after surface ΔT reached its maximum, the subcutaneous ΔT reached a maximum presumably due to the heat transferred from the surface (figure 17A). These two ΔT's decreased thereafter (see Tables 1 and 2). The colonic ΔT increased gradually after six minutes of exposure and peaked at eighteen minutes, where its rate of change was slightly greater than that of surface and subcutaneous tissue. After thirty minutes, surface, subcutaneous, and colonic rates decreased and leveled off, with the colonic ΔT still slightly above the other two. Even though the response of the core was delayed compared to surface and subcutaneous, the data suggests the increase in core ΔT and the subsequent thermoregulatory responses such as blood flow were very efficient in diminishing the ΔT in the surface and subcutaneous tissue and allowed both to stay low and fairly consistent.

The temperature data and corresponding histology of animals exposed at a power density of 75 mW/cm^2 also allowed us to define parameters where injury of the skin is expected to occur. Final surface temperatures greater than 41.5°C, final subcutaneous temperatures equal or greater than 43°C, and final colonic temperatures greater than 41°C, are predicted indicators of histological alteration (see also figure 13). It was observed that as long as the parameters defined above for surface and subcutaneous final temperatures held true, the tissue displayed injury. For example, an animal with colonic temperature less than 41°C would still show histological alteration if the surface temperature was greater than 41.5°C and subcutaneous temperature was equal or greater than 43°C. Thus, high surface and subcutaneous final temperatures and low final colonic temperatures should equal histological injury. This is presumably because if all the heat is concentrated in the outermost layers instead of being dispersed through the body (as indicated by higher colonic ΔT), there has been minimal response acting to decrease the heat load. Thermal regulation may have been overpowered.

The temperature data for animals exposed at 100 mW/cm^2 was similar to that of animals exposed to 75 mW/cm^2 for the first thirty minutes. The primary difference was that ΔT rates for 100 mW/cm^2 exposures were much more pronounced, resulting in higher peaks. As a response to the extra heat from MMW exposure at the higher power density, animals recruited heat response mechanisms (such as increased blood flow) that allowed heat transfer into and out of the body and accounted for the increase in colonic ΔT in the second fifteen-minute period of exposure. However, the rate of surface and subcutaneous ΔT began to surpass colonic rate after thirty minutes of exposure. Thus, it appears that animals exposed to 100 mW/cm^2 first responded by transferring the extra heat load out and through the body efficiently. This power density then caused heat to accumulate faster than it was being dispersed eventually overwhelming the animals' heat response mechanisms. Data from the last thirty minutes of exposure to 100 mW/cm^2 clearly show that as the rate of colonic temperature change began to decrease, extra heat began to accumulate at surface tissue. None of the animals survived the sixty-minute exposures presumably because efficient thermoregulation was overpowered.

According to Millenbaugh et al. [2006] animals exposed to 75 mW/cm^2 at 23°C ambient died at colonic temperature of 43.6°C. From our data we can conclude that animals exposed at 75 mW/cm^2 with temperatures within values greater or equal to 40.4 but less than 43.6°C will show histological insult but will survive the exposure. Also, animals exposed to 100 mW/cm^2 at 23°C ambient will show injury starting at 38.0°C colonic and die at 42.1 +/- 0.6 °C average colonic temperature. In a study by Jauchem et al. [1999] on the thermal distribution and cardiovascular effects produced by exposure to 94 GHz 75 mW/cm^2, MMW produced extreme peripheral heating without similar levels of core heating and such heating pattern of heat deposition was enough to produce circulatory failure and subsequent death. Also, Millenbaugh

et al. [2006] have recently reported that body core heating, significant only after surface and subcutaneous heating have exceeded a certain threshold of heating, is the major determinant of induction of cardiovascular collapse and death. In accordance with these studies, our data indicated that moderate core body heat transfer is necessary to restore the animal to thermal equilibrium. Our data demonstrate that heat responses at the surface, subcutaneous, and core body tissue work together to decrease MMW induced heat. However, if one of the body areas is overwhelmed by extreme heating and exceeds a temperature limit, thermoregulatory response is insufficient, leading to injury and/or death.

Post-Exposure
Histology

The value of this preliminary post-exposure study follows several paths. Examination of the histology presented us with a visual representation of the post- exposure response to MMW. As seen in animals sacrificed immediately after exposure, there is a window of variation as to whether animals will respond to MMW energy or not. While more than half of the animals exhibited high injury, the remaining animals displayed no histological alteration. Thus, it is evident that many physiological factors govern the immediate effects of MMW exposure. The ability of individual animals to throw-off heat induced by MMW may be an important factor on whether injury is experienced or not.

The histology of animals sacrificed one, two, or three day post-exposure showed two injury responses (figure 18). This suggests that a cell response occurs before a tissue response and that B responders immediately after exposure may well demonstrate changes in skin several days later. The presence of leukocyte infiltration in the tissue days later after exposure indicated an inflammatory response as the animals tried to repair injured tissue [Edlich and Drake 2005; Paul 1999]. Leukocytes became visible after one-day post-exposure, presumably as a result of inflammation and became most pronounced at three-days post-exposure in tissue showing necrotic areas (see figure 19). In studying microcirculation immediately after a burn injury and on days 1-3, 7, and 14, Langer et al. [2005] found edema and necrosis of the epidermis and partial dermis subsequent to and 24 hours post-burn. The study also found a significant increase in leukocytes adhering to the inner vessel walls immediately post-trauma and then decreasing 24 hours later possibly indicating their extensive migration into the injured tissue. Leukocytes were most pronounced 2-day post-burn. Additionally, Langer et al. found vessel dilation immediately post-burn and a return to preburn vessel diameters 3 days after burn.

The most consistent pathology finding associated with MMW exposure was the pronounced response of muscle cells associated with the panniculus carnosum. The muscle fibers pulled away from the endomysium creating an easy to detect clear space (CES). Another consistent pathology response was the change in the appearance of the dermis. The collagen of the dermis can either swell or contract in response to MMW exposure. More subtle changes in the dermis include condensation of fibroblast/fibrocyte nuclei. Dilation of blood vessels in the dermis was another common feature of tissue response to exposure. In extreme cases and at high levels of MMW exposure the dermis appeared "melted" and extravasation of blood was noted. Dermal melt may actually represent an early second-degree burn.

Tissue analysis and thresholding

Figure 20A illustrated that dermal white space for exposed skin decreased with increasing post-exposure time. This can be described in the context of necrosis observed in the tissue post-

exposure. With more post-exposure time, more necrosis was observed in the dermis. The necrosis tended to decrease the interstitial white space between collagen bundles as the dermis acquired a "melted" look. The right side served as a control for our study because it was not exposed. Thus, it was expected that no differences in the post-exposure tissue were noted. However, the increase in dermis interstitial white space in the unexposed side suggests a swelling response. This response indicates that heat generated by the exposure can find contralateral transference due either to blood flow or nervous communication. Or simply because the animal was laying on his right side during the exposure, the "right side" response may have been affected.

Figure 20B hints at the possibility of recovery as the muscle CES decreased with post-exposure time. The skin's first response to MMW may be to swell from an inflammatory response, causing the muscle white CES to increase immediately and then decrease. Thus, after a possible initial inflammatory response, the tissue slowly returned back to normal as it recovered.

Figure 20C illustrates that the dermis thickness was essentially identical when the exposed left side and the unexposed right side of skin were compared at the conclusion of the exposure. This observation must be placed into the context of panels A and B. Immediately after exposure the interstitial white space was approximately 20% greater and the muscle white space was 5 fold-different on the exposed side. As mentioned earlier, it appeared that the cellular structure was immediately affected by the exposure but not the whole tissue. Dermal swelling required more time than 60 minutes of exposure in order to become apparent. This was clearly shown as the dermis swelled considerably after given a day to recover. Since the values for dermis depth did not return to values at or below the ones observed immediately after exposure by the time the animals have been given three days to recover, one can speculate that the tissue might need more time to recover. In contrast, the dermis depth for the right side increased slightly immediately after exposure and then decreased. This suggests that the right side tissue may experience some affect, swell slightly, but then recover by three days because it was not directly exposed.

Summary

The first part of this study was aimed at tracing the path of injury development on the skin at fifteen-minute intervals of a full 60-minute exposure to 94 GHz and two power densities at 23°C ambient. Such knowledge would give information on what power density, what duration, and the amount of energy necessary to create a specific level of injury. Rather than simply concentrating on physiological data to examine the effects of MMW, we studied the histology of the exposed animals to have a visual representation of the effects of MMW on the skin and underlying tissue. The results demonstrated that heat flows from the surface to subcutaneous followed by the core body at specific time points depending on power density. Heat flow resulted in a threshold style of histological response in living animals exposed at 75 mW/cm^2, 23°C because injury was observed only after 60 minutes of exposure. In contrast, animals exposed at 100 mW/cm^2 displayed histological injury as soon as 15 minutes, which escalated with increasing exposure time, resulting in a gradient style response. The time and energy needed to reach histological change in animals exposed at 75 mW/cm^2 was 60 minutes and 270 joules of energy respectively. For 100 mW/cm^2, change was evident with the application of 90 joules at 15 minutes. The physiological response for both power densities was "gradient" in style.

In the second part the response of exposed skin after given time to recover for 1, 2, or 3 days was examined in order to determine if tissue injury became more severe or recovered. Two levels of injury response were noted in the animals: "A" responders with necrosis of the dermis and/or muscle layer and "B" responders with no injury or injury with no apparent "melt". More than half of the animals sacrificed immediately after exposure demonstrated injury representative of an A response injury. Animals sacrificed one, two, or three-day post-exposure also demonstrated A and B injury responses. The value of this preliminary post-exposure study followed several paths. First, the examination of the histology presented us with a visual representation of the post-exposure skin response to MMW. Second, the unexposed skin appeared to be affected by the left side exposures, suggesting that heat flow to the unexposed side either through the circulation or nervous system communication. Third, a cell response to MMW exposure occurs before a tissue response. Fourth, the presence of leukocyte infiltration in the tissue after exposure indicated an immune response as the animals tried to repair injured tissue. Lastly, B responders after a 60-minute exposure may well demonstrate changes in the skin several days later.

C) The effect of ambient temperature on exposure response

Observations and data collected in this study indicate that animals exposed to 94 GHz for prolonged periods at high power densities and high ambient temperatures were unable to transfer heat as efficiently as animals at lower temperatures. As a result these animals demonstrated more peripheral skin and panniculus carnosus muscle injury. It has been previously reported that the primary effect of MMW exposure is surface heating [Foster et al. 1978; Durney et al. 1986]. Indeed, 94 GHz has a tissue penetration depth of approximately 400 µm [Blick et al. 1997; Ryan et al. 2000]. Histology associated with this study revealed that the layer most sensitive to exposure at 94 GHz is the panniculus carnosus muscle layer, which is located from 700 to 1000 µm beneath the surface. Because of the shallow penetration of 94 GHz energy and the depth of the panniculus muscle, injury to this muscle layer implies that heat from exposure is rapidly transferred from the skin to this layer and the surrounding connective tissue.

A previously proposed mechanism of heat transfer from MMW exposure involves the transformation of rotational energy placed on free water molecules to kinetic energy of thermal motion [Xiao-feng and Anying 2003]. Water is a major constituent of blood, making it a good candidate for transfer of heat added from MMW exposure. It is noted that water is also the major constituent of skeletal muscle, but because of the mentioned depth of the panniculus carnosus muscle, it seems more likely that heat is transferred to blood and then to muscle. This idea is supported by the observations of Alekseev et al. [2005] who noted that increased perfusion brought about a local decrease in temperature of irradiated human skin.

Qualitative observations indicated that exposure to 94 GHz delivered at 50 mW/cm^2 at 23°C ambient had no apparent effect on exposed tissue. By thresholding images of panniculus muscle CES, quantitative data confirmed these observations (Student's T-test, n=3 for both treated and untreated sides, p=0.26). There was no significant difference in CES between exposed and unexposed side panniculus muscle tissue at this power density and ambient temperature. Prolonged exposure to 94 GHz at 50 mW/cm^2 at 33°C and 75 mW/cm^2 at both 23°C and 33°C produced significantly more clear endomysial space in muscle tissue as compared to the unexposed side tissue for these treatments (p<0.001). The increased tissue injury in animals exposed to 50 mW/cm^2 at 33°C seen in figures 22B and 23B and quantified in figure 27B supports the hypothesis that animals exposed to 94 GHz at this higher ambient

temperature could not effectively respond to heat added from the exposure. Retraction of muscle from the endomysium appears to be dependent on both power density and ambient temperature of treatment. Tissue differences attributed to ambient temperature for 50 mW/cm^2 treatment are illustrated in figure 23A, B.

For the 75 mW/cm^2 exposure at 23°C ambient, there was a large variation in percent clear endomysial space (figure 27B). Tissue exposed under this condition had a wide range of responses, from little apparent injury to the very heavy injury seen in figures 22C and 23C. It is possible that exposure to this power density at 23°C produces tissue temperatures that are near a threshold for injury. Section 1 of this study calculated such a threshold for panniculus carnosus muscle injury at a mean of surface and subcutaneous temperatures of 42.1°C. Alternatively, it might be explained by previous studies indicating that there is a very large variation in body temperature response to heat between individual rats [Furuyama et al. 1984]. A larger number of animals for this treatment might further elucidate this phenomenon.

The high level of CES seen in panels C and D of figure 23 appears in conjunction with vasodilation and extravasation. It has been previously reported that during longer exposures skin blood flow increased due to heating of cutaneous vasculature [Nelson et al. 2003; Walters et al. 2004]. Heat, then, would be most concentrated at or near the penetration depth of 94 GHz. The observed vasodilatation implies increased blood flow to the area of high heat concentration, likely in a physiological attempt to channel heat away to areas that can effectively disperse it. Heat transferred by blood is likely responsible for the injury seen in the panniculus carnosus muscle.

The effects of prolonged MMW exposure on adipose tissue and the surrounding vasculature are illustrated in figure 24. All treatments except for the 50 mW/cm^2 at 23°C displayed extreme vasodilation and extravasation. Displayed in figure 24B is an example of adipocyte ruffling, likely from injury due to MMW exposure. There was no consistent trend observed in how adipose tissue was affected by exposure. Epidermal tissue examined was similarly inconclusive.

Rather than to focus on the amount of time of exposure, it proved helpful to consider the amount of energy that had been applied to experimental animals. This was especially beneficial in ascertaining the differences between exposures at the same ambient temperature but at different power densities. The linear increase in the difference in colonic temperatures for animals at different ambient temperatures seen in figure 26 implies that as energy was applied, it was carried away from the exposure site to other areas and eventually caused an increase in core body temperature. It has been previously reported that core heating from MMW exposure is the primary cause for circulatory collapse leading to death in exposed animals [Jauchem et al. 1999; Millenbaugh et al. 2006].

It was expected that, because at an ambient temperature of 33°C rats cannot effectively thermoregulate, there would be an increase in the difference in temperature as more energy was applied to experimental animals. As more energy was applied, this difference in temperature was representative of heat that the exposed animals were unable to effectively disperse at 33°C in comparison to 23°C. Energy was applied more quickly at 75 mW/cm^2 as compared to 50 mW/cm^2 which likely contributed to the reduced time-to-death in 75 mW/cm^2 treated animals at 33°C. Panels A and B of figure 26 display a short but distinct decrease in the difference of surface temperatures. In figure 26A it was observed after approximately 120 J/cm^2 had been applied and in figure 26B it was observed after approximately 50 J/cm^2 had been applied. This decrease could be representative of the activation or more efficient use of a large heat dispersal

mechanism, such as the tail. The tail can act as a heat-sink due to its lack of coarse hair, large surface area, and the autonomic control of blood flow to it [Dawson and Keber 1979; Berry et al. 1984]. The appearance of the results of such a mechanism at the smaller applied energy (and thus a shorter time of exposure) seen in figure 26B could be explained by the fact that energy in 75 mW/cm^2 treated animals was applied more quickly than in 50 mW/cm^2 treated animals. In figure 26 panel C, it was observed that, at 33°C ambient, there was approximately zero difference in colonic temperatures as similar amounts of energy had been applied regardless of power density. This result was expected of animals that could not effectively remove heat through radiation, convection, and conduction due to the high ambient temperature [Gordon 1990].

At time of death, the average colonic temperature difference between 50 mW/cm^2 23° and 33°C treated animals was 4.4°C and between 75 mW/cm^2 23°C and 33°C treated animals was 4.2°C. The slightly higher temperature difference in the 50 mW/cm^2 treated animals can be explained by the fact that these animals had more energy applied to them before death than did the 75 mW/cm^2 treated animals (196.7 J/cm^2 compared to 188 J/cm^2). The 4.2°C and 4.4°C colonic temperature differences represent the heat that could not be removed by 33°C exposed rats over the course of the exposure and until death.

Generally, dermis interstitium decreased when exposures took place at 33°C (figure 27A). However, the only significant difference in dermis collagen spacing that could be confirmed through thresholding analysis was between the 50 mW/cm^2 33°C and 75 mW/cm^2 23°C conditions. Panniculus carnosus muscle fiber retraction from the endomysium, however, proved to be significantly different between animals exposed to 50 mW/cm^2 at 23°C and all other treatments. The effect of ambient temperature is displayed through treatments at 33°C ambient, which showed the highest average percent clear endomysial space. While 50 mW/cm^2 treatment at 23°C seemed to produce no significant effect, 75 mW/cm^2 treatment at this same temperature showed a variable effect of little to much tissue injury. The variation for this treatment is depicted in figure 27B.

Ambient temperature has a profound effect on the heat-response capability of MMW exposed rats. At 33°C, 94 GHz exposed rats cannot shed heat as effectively as rats exposed at 23°C. This leads to increased tissue injury, especially in the panniculus carnosus muscle layer, and eventual death.

D and E) The effect of anesthesia on exposure response and passive heating effects

It does appear that isoflurane anesthesia induces vasodilation or perhaps stops vasoconstriction of the peripheral thermal compartment of the rat. As a result the anesthetized rat body temperature drops by about 3°C during the course of an hour (see figure 28). The anesthesia temperature compensated rat demonstrated a 2°C temperature elevation higher than the uncompensated rat. The uncompensated rat in terms of anesthesia-induced hypothermia was the norm for MMW exposures performed during this project. This phenomenon requires further investigation.

Only very early steps were taken to analyze passively heated dead rats. The dead animal has no vascular or nervous system interplay in terms of thermoregulation. A critical comparison of passively heated dead rats with thermoregulating exposed rats could yield interesting insights into the thermoregulation process.

F) Thermograph correlation to histology

The Gaussian distribution of MMW energy to the surface of the rat offers problems as well as opportunities. In terms of problems the skin and body contours of the rat perturb the expected distribution of surface heat to the animal. Not only is the skin depth not homogeneous in terms of layers with different dielectric properties, but the surface area of the skin varies as well. In terms of modeling thermal flow through skin, the question becomes which skin should serve as the baseline. As an opportunity the Gaussian distribution of energy produces a mosaic of power densities over the surface. Several power densities could be studied in one large histological sample in the same animal, assuming that variations in the skin can be accounted.

An explanation of the variances in the thermographs would be quite instructive for future studies.

G) Modeling MMW induced heat flow through skin

Most thermal models that treat the heterogeneous nature of skin exposed to MMW have the highest levels of heat associated with the epidermis. Dielectric interfaces between dermal, subcutaneous, epidermal, and muscle are given great credence in these models (see figure 32). However, most models do not know how to treat the actual deposition of heat within the tissue. It is generally accepted that MMW heats the tissue from the inside out, albeit only about 0.4 to 0.8 mm deep, in contrast to a burn, which is from the outside in.

Blood perfusion poses the most identifiable physiological process that moves deposited energy and heat within the skin tissue and to the body core. The modifying effects of the nervous system are generally overlooked. Investigators such as Weaver et al. look for substances that are elaborated through the exposed tissue (see figure 35). How should models deal with this?

Perhaps the only approach is to look at IR data from the cut surface of the skin. By magnifying the cut skin surface to the IR camera, one could actually watch heat flow into the depth of the skin. This is no small task and is the subject for future research.

References:

Adair ER, Spiers DE, Rawson RO, Adams BW, Sheldon DK, Pivirotto PH, Akel GM. 1985. Thermoregulatory consequences of long-term microwave exposure at controlled ambient temperatures. Bioelectromagnetics 6(4):339-363.

Adair ER, Petersen RC. 2002. Biological effects of radio-frequency/microwaves radiation. IEEE Transactions on Microwave Theory and Techniques 50:953-962.

Adair ER, Black DR. 2003. Thermoregulatory responses to RF energy absorption. Bioelectromagnetics 24(6):S17-S38.

Alekseev SI, Radzievsky AA, Szabo I, Ziskin MC. 2005. Local heating of human skin by millimeter waves: effect of blood flow. Bioelectromagnetics 26:489-501.

Aulick LH, Wilmore WW, Mason AD, Pruitt BA. 1978. Muscle blood flow following thermal injury. Annals of Surgery 188(6):778-82.

Berry JJ, Montgomery LD, Williams BA. 1984. Thermoregulatory responses of rats to varying environmental temperatures. Aviation, Space, and Environmental Medicine. 55(6):546-549.

Blick DW, Adair ER, Hurt WD, Sherry CJ, Walters TJ, Merritt JH. 1997. Thresholds of microwave-evoked warmth sensations in human skin. Bioelectromagnetics 18(6):403-409.

Budd RA. 1985. Can microwave/radiofrequency radiation (MMW) burns be distinguished from conventional burns? Journal of Microwave Power 20(1):9-11.

Charkoudian N. 2003. Skin blood flow in adult human thermoregulation: how it works, when it does not, and why. Mayo Clinic Proceedings 78(5):603-612.

Chase HB, Montagna W, Malone JD. 1953 Changes in the skin in relation to the hair growth cycle. Anatomy Records 116(1):75-81.

Clark AS, Kelly RA, Mitch WE. 1984. Systemic response to thermal injury in rats: accelerated protein degredation and altered glucose utilization in muscle. Journal of Clinical Investigation 74(3):888-897.

Dawson NJ, Keber AW. 1979. Physiology of heat loss from an extremity: the tail of the rat. Clinical and Experimental Pharmacology & Physiology 6(1):69-80.

Diller KR, Ryan TP. Heat transfer in living systems: current opportunities. Journal of Heat Transfer 120:810-827.

Durney CH, Massoudi H, Iskander MF. 1986. Radiofrequency Radiation Dosimetry Handbook, 4th ed. Brooks Air Force Base, Texas: US Air Force School of Aerospace Medicine, Technical Report USAFSAM 85-73.

Edlich RF, Drake DB. 2005. Thermal burns. eMedicine [online]. Available from: http://www.emedicine.com/plastic/tpic518.htm.

Erwin D. 1983. An overview of the biological effects of radiofrequency radiation. Military Medicine 148(2):113-117.

Ferguson MK, Seifert FC, Replogle RL. 1982. The effects of thermal injury on rat skeletal muscle microcirculation. The Journal of Trauma 22(10):880-883.

Foster KR, Kritikos HN, Schwan HP. 1978. Effect of surface cooling and blood flow on the microwave heating of tissue. IEEE Transactions on Bio-medical Engineering 25(3): 313-316.

Frei MR, Ryan KL, Berger RE, Jauchem JR. 1995. Sustained 35 GHz radiofrequency irradiation induces circulatory failure. Shock 4(4):289-293

Fuyurama F, Ohara K, Ota A. 1984. Estimation of rat thermoregulatory ability based on body temperature response to heat. Journal of Applied Phyiology: Respiratory, Environmental and Exercise Physiology 57(4):1271-1275.

Gordon CJ, Ali JS. 1987. Comparative thermoregulatory response to passive heat loading by exposure to radiofrequency radiation. Comparative Biochemistry and Physiology A 88(1):107-112.

Gordon CJ. 1990. Thermal biology of the laboratory rat. Physiology & Behavior 47(5):963-991.

Gowrishankar TR, Stewart DA, Martin GT, Weaver JC. 2004. Transport lattice models of heat transport in skin with spatially heterogeneous, temperature-dependent perfusion. BioMedical Engineering OnLine 3:42. Available from: http://www.pubmedcentral.gov/articlerender.fcgi?tool=pubmed&pubmedid= 15548324.

IEEE Std C95.1-2005, IEEE Standard for Safety Levels with Respect to Human Exposure to Radio Frequency Electromagnetic Fields, 3 kHz to 300 GHz.

Jauchem JR, Ryan KL, Frei MR. 1999. Cardiovascular and thermal responses in rats during 94 GHz irradiation. Bioelectromagnetics 20(4):264-267.

Jauchem JR. 2006. The role of autacoids and autonomic nervous system in cardiovascular responses to radio-frequency energy heating. Autonomic and Autocoid Pharmacology 26(2):121-140.

Johnson CC, Guy AW. 1972. Nonionizing electromagnetic wave effects in biological materials and systems. IEEE Proceedings 60(6):692-718.

Kurz A, Sessler DI, Narzt E. 1995. Morphometric influences on intraoperative core temperature changes. Anesthesia and Analgesia 80:562-567.

Langer S, Goertz O, Steinstraesser L, Kuhnen C, Steinau HU, Homann HH. 2005. New model for in vivo investigation after microvascular breakdown in burns: use of intravital fluorescent microscopy. Burns 31:168-174.

Lenhardt R, Greif R, Sessler DI, Laciny S, Rajek A, Bastanmehr H. 1999. Relative contribution of skin and core temperatures to vasoconstriction and shivering thresholds during isoflurane anesthesia. Anesthesiology 91:422-9.

Millenbaugh NJ, Kiel JL, Ryan KL, Blystone RV, Kalns JE, Brott BJ, Cerna CZ, Lawrence WS, Soza LL, Mason PA. 2006. Comparison of blood pressure and thermal responses in rats exposed to millimeter wave energy or environmental heating. Shock 25:625-632.

Nelson DA, Nelson MT, Walters TJ, Mason PA. 2000. Skin heating effects of millimeter-wave irradiation-thermal modeling results. IEEE Transactions on Microwave Theory and Techniques 48(11):2111-2120.

Nelson DA, Walters DJ, Ryan KL, Emerton KB, Hurt WD, Ziriax JM, Johnson LR, Mason PA. 2003. Inter-species extrapolation of skin heating resulting from millimeter wave irradiation: modeling and experimental results. Health Physics 84(5):608-615.

Odessey R, Parr B.1982. Effect of insulin and leucine on protein turnover in rat soleus muscle after burn injury. Metabolism 31(1):82-87.

Pakhomov AG, Akyel Y, Pakhomova ON, Stuck BE, Murphy MR. 1998. Current state and implications of research on biological effects of millimeter waves: A review of the literature. Bioelectromagnetics 19:393-413.

Paul WE, editor. 1999. Fundamental Immunology, 4th ed. Philadelphia: Lippincott-Raven Publishers. Pgs. 1051-1061.

Prophet E. 1994. Tissue processing: dehydration, clearing, and infiltration in Eds. Prophet E, Mills B, Arrington JB, Sobin LH. Armed Forces Institute of Pathology Laboratory Methods in Histotechnology. ISBN:1-881041-00-X pg. 29.

Rand RP, Burton AC, Ing T. 1965. The tail of the rat, in temperature regulation and acclimatization. Canadian Journal of Physiology and Pharmacology 43:257-267.

Roberts NJ, Michaelson SM, Lu S. 1986. The biological effects of radiofrequency radiation: a critical review and recommendations. International Journal of Radiation Biology 50:379-420.

Ryan KL, D'Andrea JA, Jauchem JR, Mason PA. 2000. Radio frequency radiation of millimeter wave length: potential occupational safety issues related to surface heating. Health Physics 78(2):170-181.

Sessler DI. 2000. Perioperative heat balance. Anesthesiology 92:578-96.

Stewart DA, Gowrishankar TR, Weaver JC. 2006. Skin heating and injury by prolonged millimeter wave exposure: theory based on a skin model coupled to a whole body model and local biochemical release from cells at supraphysiologic temperatures. IEEE Transactions on Plasma Science 34(4):1-13.

Thomas JR. 2005. Effects of age and diet on rat skin histology. Laryngoscope 115(3):405-411.

Walters TJ, Ryan KL, Nelson DA, Blick DW, Mason PA. 2004. Effects of blood flow on skin eating induced by millimeter wave irradiation in humans. Health Physics 86(2):115-120.

Weiss J, Taylor GR, Zimmermann F, Nebendahl K. 2000. The collection of body fluids. Ed.
        Krinke GJ. The laboratory rat. ISBN:0-12-426400-X pg. 491.
Xiao-feng P, Anying Z. 2003. Mechanisms of thermally biological effects of the
        millimeter waves and its properties. International Journal of Infrared and Millimeter
        Waves 24: 1899-1912.
Young AA, Dawson NJ. 1982. Evidence for on-off control of heat dissipation from the tail of the
        rat. Canadian Journal of Physiology and Pharmacology 60(3):392-398.